J. Fluid Mech. (1981), *vol.* 113, *pp.* 91–122
Printed in Great Britain

Equilibrium boundary layers in moderate to strong adverse pressure gradients

By W. H. SCHOFIELD
Aeronautical Research Laboratories, Fishermen's Bend, Melbourne, Australia

(Received 1 October 1980 and in revised form 15 April 1981)

An analysis of equilibrium boundary layers based on the Schofield–Perry defect law, which applies to flow in a moderate to strong adverse pressure gradient, is presented. The conditions derived for self-preserving or equilibrium boundary layers differ from those given by previous analyses based on the usual velocity-defect law. It is shown that twelve observed boundary layers on smooth walls conform to these new conditions for precise equilibrium flow. As the analytical expression for the Schofield–Perry defect law does not vary with pressure gradient, a specific expression for the shear-stress profile in any equilibrium layer can be derived. The predicted shear-stress profiles show good agreement with experimental data. Limits for the flow parameters within which equilibrium layers can exist are derived, and it is shown that observed equilibrium layers fall within these limits. A prediction method for layers in smoothly changing adverse-pressure gradients is outlined and demonstrated using equilibrium data. The unified account of equilibrium flow in adverse pressure gradients presented here is used to resolve some disagreements in the literature concerning existence conditions for equilibrium boundary layers.

1. Introduction

The numerous papers that have been published on turbulent boundary layers developing in adverse pressure gradients attest both the engineering significance of the problem and its intractability. A review of this literature does not inspire hope that a general analysis of these flows will be available in the near future. A central difficulty in attempting any such analysis is that the outer region of a turbulent boundary layer possesses a complex nonlinear memory of events upstream and hence velocity distributions at any position depend on both upstream as well as local conditions. To reduce the complexity of the problem Clauser (1954) set out to study a subset of adverse-pressure-gradient boundary layers that had a constant force history and could thus be described by local parameters alone. As the external forces acting on a boundary layer arise from the pressure gradient dp/dx and the wall shear stress τ_0, a layer with a constant force history (an equilibrium layer) was conceived by Clauser as a layer in which the non-dimensional force ratio

$$\beta_c = (\delta^* dp/dx)/\tau_0$$

(where δ^* is the displacement thickness of the boundary layer) was held constant throughout the layer's development. Clauser expected such equilibrium layers to be

dynamically similar at all stations in both the mean and fluctuating velocity fields.† Clauser did not, however, use this force ratio to set up his experimental flows. He worked instead by analogy from the only equilibrium layer that was then known, the zero-pressure-gradient layer where $\beta_c = 0$ as $dp/dx = 0$. It was well established that for this case the mean-velocity-defect law

$$(U_1 - u)/u_\tau = \phi(y/\delta) \tag{1}$$

(where U_1 is the free-stream velocity, δ the total layer thickness, ρ is the fluid density and $u_\tau = \tau_0^{\frac{1}{2}}\rho^{-\frac{1}{2}}$) accurately described the mean velocity from the free stream down almost to the wall. Clauser reasoned that a defect law of the same form should apply to equilibrium layers in pressure-gradient flows. Therefore Clauser adjusted the pressure gradient acting on a two-dimensional boundary layer until mean flow profiles along the layer agreed with an equation in the defect form of equation (1). Two such layers in adverse pressure gradient were produced. By defining equilibrium layers in terms of equation (1) Clauser tacitly assumed that the length and velocity scales for zero-pressure-gradient flow (δ, u_τ) were the relevant scales for equilibrium layers in adverse-pressure-gradient flow. Later work showed that this assumption causes analytical and conceptual difficulties for equilibrium layers near separation where u_τ approaches zero.

Townsend analysed Clauser's flows in the first of a series of important papers (Townsend 1956*a*, *b*, 1960, 1961*a*, *b*, 1965*a*, *b*) in which his self-preserving‡ flow analysis was developed. In this analysis self-preserving forms for the mean and fluctuating components are assumed, so that

$$u = U_1 + u_0 f(y/l_0), \quad \overline{u'v'} = u_0^2\, g(y/l_0), \quad \overline{u'^2} = u_0^2 h(y/l_0), \tag{2}$$

etc., where primes denote fluctuating quantities and u_0 and l_0 are (as yet) undefined velocity and length scales of the flow. These relations are substituted into the equation of motion, § and for self-preserving flow to be possible it is necessary that in the resulting equation the coefficients of the various terms should either be zero or proportional to each other, i.e. it must be possible to remove x from the equation. This stipulation produces relationships between l_0, u_0 and x, U_1 which are the conditions for self-preserving flow. Both Townsend (1956*a*, *b*, 1961*a*, *b*) and Rotta (1962) have applied this method to boundary-layer flow in adverse pressure gradients. A good summary of these results and their implications is given by Rotta who took the length and velocity scales as $\delta^* U_1/u_\tau$ and u_τ, respectively, and showed that the conditions for self-preserving flow were

$$u_\tau/U_1 = \text{const.}, \quad d\delta/dx = \text{const.}, \tag{3a, b}$$

with the corollary

$$\beta_c = \text{const.} \tag{3c}$$

Equation (3*c*) implies that these self-preserving layers are the equilibrium layers that were originally conceived by Clauser. Rotta (1962) lists six combinations of pressure

† The small eddy end of the turbulence spectrum was to be excluded from this dynamic similarity.

‡ Townsend reserves the term 'equilibrium' to describe a different property of turbulent flow, see Townsend (1976, p. 139).

§ To make the analysis possible, viscous and normal stress terms are omitted from the equations of motion, implying accuracy only at high Reynolds numbers.

gradient and wall-roughness distribution that will satisfy equation (3). The listing shows that adverse-pressure-gradient equilibrium layers require a free-stream velocity variation of the form

$$U_1 = a(x-x_0)^m \quad (m < 0). \tag{4}$$

Stratford (1959) reported measurements in boundary layers which were held at incipient separation. These flows are of considerable theoretical interest because if $u_\tau = 0$ then $\beta_c = \infty$, which is a limiting case for equilibrium layers. Stratford claimed that his mean velocity profiles near the wall did not contain a logarithmic region† but correlated instead with a half-power law of the form

$$u = \text{const.}\,(\alpha y)^{\frac{1}{2}} + \text{const.}\,(\alpha\nu)^{\frac{1}{3}}, \tag{5}$$

where $\alpha = (1/\rho)\,dp/dx$ and ν is the kinematic viscosity of the fluid.

Townsend (1960, 1961*b*, 1976) and Mellor & Gibson (1966) have both presented analyses of equilibrium layers in adverse pressure gradients which include the limiting case $\beta_c = \infty$. These analyses show that the use of u_τ as the velocity scale for equilibrium layers presents serious problems for layers with values of u_τ near zero. Firstly, as $u_\tau \to 0$ the logarithmic law of the wall, which forms the inner portion of the flow description, disappears. Secondly, the question arises: what does a defect law given by equation (1) mean for the case $u_\tau = 0$? These difficulties were overcome by adopting a new velocity scale for analysing equilibrium layers in strong adverse pressure gradients. This velocity scale was based on α mainly because Stratford's experimental results for layers near separation suggested that mean velocity near the wall depended on α. Thus Mellor & Gibson (1966) and Townsend (1960, 1961*b*, 1976) using

$$u_P = (\alpha\delta^*)^{\frac{1}{2}}, \tag{6}$$

and Kader & Yaglom (1978) and Yaglom (1979) using

$$u_P = (\alpha\delta)^{\frac{1}{2}}$$

and various closure hypotheses, were able to analyse near-separating equilibrium layers. These and other authors have arrived at specific conclusions concerning the nature of equilibrium flow and the limits in flow parameters for the existence of equilibrium layers. These conclusions show significant disagreements on the following points:

(i) the limits of m within which equilibrium layers can exist;

(ii) the number of equilibrium layers that can exist for a given set of initial and boundary conditions;

(iii) the relationship between m and the velocity scale ratio (u_0/U_1) of an equilibrium layer;

(iv) the appropriate velocity scale for equilibrium layers near separation.

Townsend (1960, 1961*b*, 1976) calculates that, for a given set of initial and boundary conditions, two different equilibrium layers are possible if $m < -0{\cdot}25$. However, he also notes (Townsend 1976, p. 279) that experimental results indicate that two equilibrium layers can apparently exist for m near $-0{\cdot}23$, which is numerically smaller than his calculated limit. The calculations also show that the smallest value

† Detailed analysis by Coles & Hirst (1968) showed however that most of his layers did have small logarithmic regions and the wall shearing stress, although small, was not zero.

of m for which an equilibrium layer can exist depends on Reynolds number and is $-\frac{1}{3}$ for an infinite Reynolds number increasing to $-0{\cdot}28$ for a Reynolds number of 10^{11}. Similarly, East, Sawyer & Nash (1979) present results from an approximate analytic solution given by East, Smith & Merryman (1977), that suggest:

(i) two different equilibrium layers are possible for $m < 0$;

(ii) the smallest value of m for which an equilibrium layer can exist is Reynolds-number-dependent. (For a momentum-thickness Reynolds number of 10^6 the limit is $m = -0{\cdot}27$.)

In contrast are Mellor & Gibson's (1966) calculations which predict a single sequence of equilibrium layers terminating at $m = -0{\cdot}23$. These authors also develop a relationship between the integral thickness of an equilibrium layer and m which implies an (effectively) unique relationship between velocity-scale ratio u_0/U_1 and m. Mellor in 1966 disputed Townsend's result that for a given set of conditions two equilibrium layers were possible. In this he was joined by Bradshaw (1966) who attributed the result to Townsend's assumption of a smooth join between two approximate analytical solutions for the inner and outer regions. Bradshaw states that, although both solutions are good approximations far from the join, the assumption is unlikely to be accurate at the join for layers with large velocity defects. He concludes that on the balance of probabilities only one equilibrium boundary layer can exist in a given pressure gradient. Bradshaw supports this conclusion in a later paper (Bradshaw 1967) that presents calculations which use the method of Bradshaw, Ferriss & Atwell (1967). These suggest that for $m = -0{\cdot}255$ the same equilibrium condition is arrived at by a range of layers which start with the same value of $U_1\theta/\nu$ (where θ is the momentum thickness of the layer) at different streamwise stations. The calculations also show that no equilibrium layer is possible for $m < -0{\cdot}3$. Head (1976), however, considers that if the experimental evidence is taken at face value it would suggest that a whole range of equilibrium layers should exist for m near $-0{\cdot}25$. He supports this with another set of calculations that suggests:

(i) for $m = -0{\cdot}35$ no equilibrium layer is possible;

(ii) for $m = -0{\cdot}15$ only one equilibrium layer is possible irrespective of initial conditions;

(iii) for $m = -0{\cdot}255$ a range of equilibrium layers is possible depending on the initial conditions of the layer. For this case, the calculations show that if the initial value of $U_1\theta/\nu$ is sufficiently large then the equilibrium layer will separate.

The analysis presented here leads to a comprehensive account of equilibrium layers in adverse pressure gradients which helps to resolve many of these disagreements.

A central thesis of this analysis is that both u_τ and velocity scales based on α are inappropriate for layers in moderate to strong adverse pressure gradients. Historically, α was first used to describe layers near separation because Stratford's results appeared to show that in these layers equation (5) replaced the logarithmic law in describing mean flow near the wall. However, it has been shown subsequently that equation (5) cannot describe all the half-power distributions that have been observed in adverse-pressure-gradient layers in the region adjacent to the logarithmic law (Schofield & Perry 1972; Perry & Schofield 1973; Kader & Yaglom 1978; Yaglom 1979). Thus equation (5) is not valid in all cases.

Another argument in favour of velocity scales based on α that is often advanced (e.g. Stratford 1959, p. 3; Kader & Yaglom 1978, p. 310) starts by observing that near

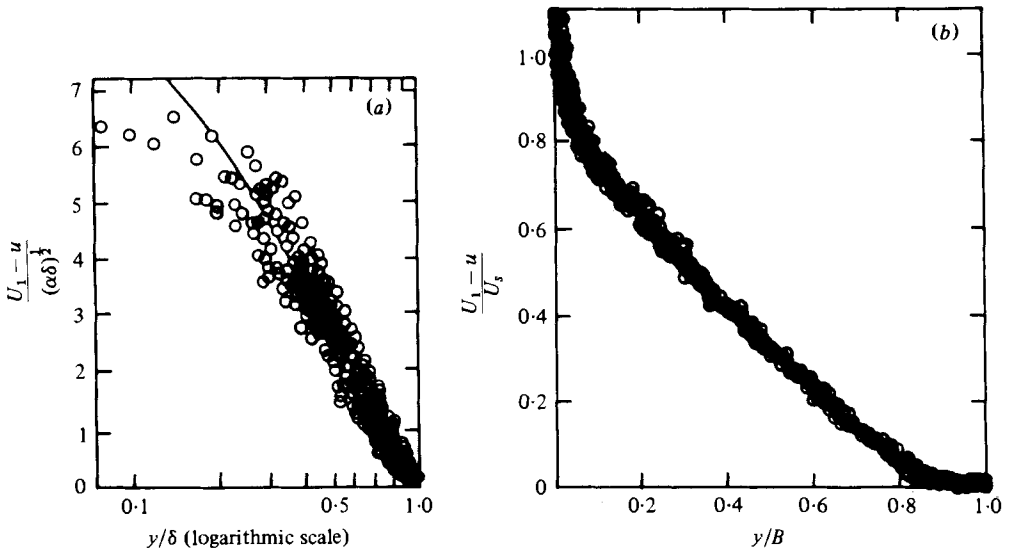

FIGURE 1. Defect laws for boundary layers in adverse-pressure-gradient flows. (*a*) Kader–Yaglom defect law (taken from Kader & Yaglom 1978). (*b*) Schofield–Perry defect law (from Schofield & Perry 1972, also Perry & Schofield 1973).

the wall of a boundary layer where inertia forces are small the equation of motion can be approximated by

$$\tau \simeq \tau_0 + \rho\alpha y. \tag{7}$$

In a strong adverse-pressure-gradient layer α is large and τ_0 is small; thus at small distances from the wall τ is largely determined by $\rho\alpha y$ rather than τ_0. It is then postulated that the mean velocity at small distances from the wall will also depend on α rather than τ_0, which does not necessarily follow. Indeed if τ_0, which is a measure of the boundary layer's response to its initial and boundary conditions, determines the mean velocity distributions in the viscous and logarithmic regions, it seems improbable that in the adjacent half-power region it should be replaced by α which is a different type of variable, being one of the layer's boundary conditions. It would seem more plausible to replace τ_0 with another boundary-layer-response variable. The present analysis does this by using a velocity scale U_m which is related to the maximum shear stress in the layer, τ_m, namely

$$U_m = (\tau_m/\rho)^{\frac{1}{2}}. \tag{8}$$

This velocity scale has several factors in its favour. It is the velocity scale of a half-power law which accurately describes all the half-power distributions that have been observed in moderate to strong adverse-pressure-gradient layers (Perry & Schofield 1973). This half-power law is the innermost portion of a universal velocity-defect law for adverse-pressure-gradient layers which describes the mean flow from the free stream almost to the wall. Its validity has been demonstrated in Schofield & Perry (1972), Perry & Schofield (1973), Simpson, Strickland & Barr (1977), Samuel (1973), Samuel & Joubert (1974), Fairlie (1973), Perry & Fairlie (1975), and is further demonstrated in this paper. Unlike equation (1) and the various defect laws based on u_P, the Schofield–Perry defect law has an invariant analytical form for all adverse pressure

gradients. Its validity is restricted to adverse pressure gradients sufficiently strong for $\tau_m \geqslant \frac{3}{2}\tau_0$ approximately (Perry & Schofield 1973). Thus the analysis presented here is also restricted to equilibrium layers in which $\tau_m \geqslant \frac{3}{2}\tau_0$ approximately.

The analysis gives:

(i) limits for the existence of equilibrium layers which relate to the initial and boundary conditions of the equilibrium layer;

(ii) an explicit analytical function for the shear-stress profile of any equilibrium layer;

(iii) a simple method for prediction of the mean flow field of equilibrium layers.

The results of the analysis represent an improvement on some aspects of the recent work by Kader & Yaglom (1978), who retain α as a variable in their defect law for adverse-pressure-gradient layers. By retaining α, their analytical description of the mean profile requires a set of complicated equations separated by complex blending functions. Also the Kader–Yaglom defect law does not describe the data as accurately as the Schofield–Perry defect law does (see figure 1). It is to be noted that if, in the dimensional analysis on which Kader & Yaglom's work is based, $\alpha\delta$ had been replaced by U_m^2, the Schofield–Perry relations could have been derived.

2. Similarity laws in zero- and adverse-pressure-gradient boundary layers

The accepted model for two-dimensional turbulent boundary layers in zero-pressure-gradient flow is a viscous sublayer immediately adjacent to the wall blending into the logarithmic law of the wall,

$$\frac{u}{u_\tau} = \frac{1}{\kappa}\ln\frac{yu_\tau}{\nu} + A, \tag{9}$$

where κ, A are universal constants. The logarithmic law forms the innermost portion of a velocity-defect law which describes the mean profile from the sublayer edge to the free stream. This defect law is described by the expression

$$\frac{U_1 - u}{u_\tau} = 9{\cdot}6(1 - y/\Delta)^2 \tag{10}$$

(where $\Delta = 0{\cdot}3\delta^* U_1/u_\tau$ is an integral layer thickness) over the full range of its validity (Hama 1954).

The model proposed by Schofield & Perry is similar in form to this but applies to attached boundary layers in moderate to strong adverse pressure gradients (specifically layers in which $\tau_m \geqslant \frac{3}{2}\tau_0$). The model consists of the same viscous sublayer and (a smaller) logarithmic law that tangentially joins the half-power law,

$$\frac{u}{U_1} = 0{\cdot}8\left(\frac{yU_m^2}{LU_1^2}\right)^{\frac{1}{2}} + 1 - \frac{U_s}{U_1} \tag{11a}$$

$$= 0{\cdot}47\left(\frac{U_s}{U_1}\right)^{\frac{3}{2}}\left(\frac{y}{\delta^*}\right)^{\frac{1}{2}} + 1 - \frac{U_s}{U_1}, \tag{11b}$$

where L is the distance from the wall to τ_m and U_s is a velocity scale. This half-power law forms the innermost portion of a velocity-defect law which describes the mean

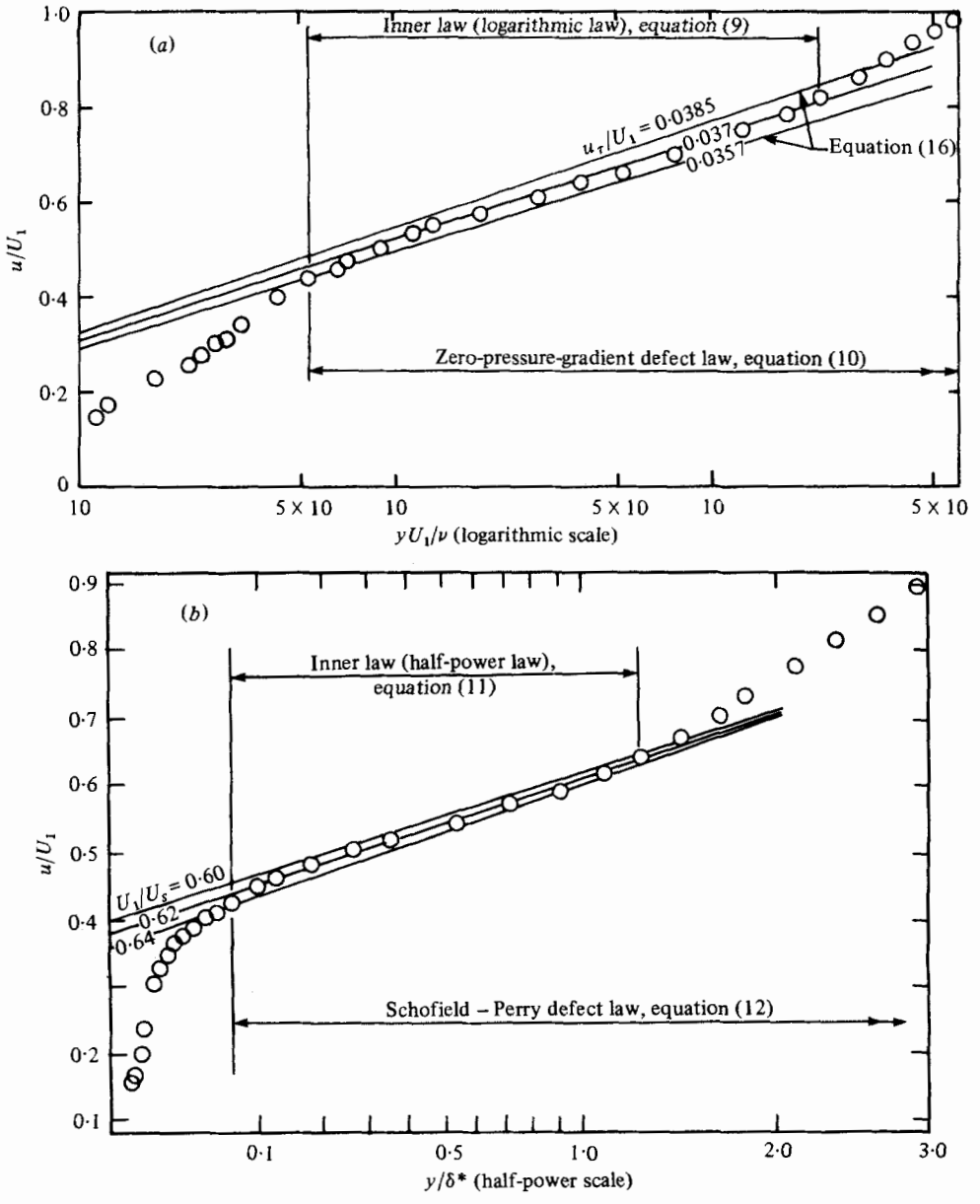

FIGURE 2. Similarity laws for boundary layers. (*a*) Zero-pressure-gradient flow: ○, Klebanoff (1954). (*b*) Adverse-pressure-gradient flow: ○, Bradshaw & Ferriss (1965).

profile from very near the wall out to the free stream. This defect law is accurately described by the expression

$$\frac{U_1-u}{U_s} = 1-0{\cdot}4\left(\frac{y}{B}\right)^{\frac{1}{2}} - 0{\cdot}6\sin\left(\frac{\pi y}{2B}\right) = f\left(\frac{y}{B}\right) \tag{12}$$

(where $B = 2{\cdot}86\delta^*U_1/U_s$ is an integral layer thickness) over the full range of its validity. U_s is a velocity scale found by extrapolating the half-power law to the wall and is related (Perry & Schofield 1973) to the velocity scale by

$$U_s = 8(B/L)^{\frac{1}{2}}U_m, \tag{13}$$

which is a notable equation in as much as it relates mean-flow parameters to a turbulent-flow parameter.

Perry & Schofield (1973) have also shown that the distance from the wall to the tangential junction of the logarithmic layer and the half-power layer (y_c) is given by

$$y_c = 37{\cdot}1u_\tau^2 B/U_s^2, \tag{14}$$

from which it follows that

$$y_c = 18{\cdot}6c_f' BU_1^2/U_s^2. \tag{15}$$

Thus, for a boundary layer held at incipient separation where $c_f' = 0$, equation (15) gives $y_c = 0$, implying no logarithmic layer and a half-power layer that extends to the wall.† The disappearance of the logarithmic region as separation is approached is consistent with Stratford's results and with the well-known observation that the vertical height of the logarithmic region decreases as the strength of an adverse pressure gradient increases. The boundary layers considered in this report are all in moderate to strong adverse pressure gradient and hence have small logarithmic regions with half-power regions extending close to the wall. Consequently the Schofield–Perry model accurately described their mean-flow profiles from the free stream down to a few per cent of layer thickness from the wall (see figures 2*b*, 5 and 7). It is the basis for the analysis presented in § 3.

The velocity scale appearing in the Schofield–Perry defect law, can be determined from the mean profile by adapting Clauser's methodology to the half-power law. The Clauser (1954) method determines the velocity-scale ratio (u_τ/U_1) from the logarithmic law by rewriting equation (9) as

$$\frac{u}{U_1} = \frac{u_\tau}{\kappa U_1}\ln\frac{yU_1}{\nu} + \frac{u_\tau}{\kappa U_1}\ln\frac{u_\tau}{U_1} + \frac{u_\tau}{U_1}A, \tag{16}$$

plotting the mean profile on co-ordinates u/U_1, $\ln(yU_1/\nu)$ and comparing it with the family of straight lines for different values of u_τ/U_1 as illustrated in figure 2(*a*). In a similar manner the velocity scale ratio U_s/U_1 can be determined from equation (11*b*). The mean profile is plotted on co-ordinates u/U_1, $(y/\delta^*)^{\frac{1}{2}}$ and is compared with the family of straight lines for different values of U_s/U_1, as illustrated in figure 2(*b*).

3. Analysis

Consider a two-dimensional turbulent boundary layer in an adverse pressure gradient which is sufficiently strong for $\tau_m \geqslant \frac{3}{2}\tau_0$ at all streamwise positions. For such a layer the Schofield–Perry defect law will give an accurate description of the mean profile from the free stream down to a small distance from the wall.‡ Following the self-preserving analysis detailed in Townsend (1976) and Rotta (1962), self-preserving forms for the mean and fluctuating flow components are assumed using Schofield–Perry velocity and length scales, namely

$$u = U_1 - U_s f(y/B), \tag{12}$$

† Obviously this is only approximate as no account of the viscous sublayer has been taken.

‡ Experimental results from a variety of boundary layers indicate that this distance varies between about 1 and 4 per cent of total layer thickness.

where the analytic fit to f has been given above, and

$$\overline{u'v'} = U_s^2 g(y/B). \tag{17}$$

These relations are substituted into the equation of mean motion in which the viscous and normal stress terms have been omitted. The continuity equation is first used to eliminate the mean vertical velocity and then integration of the equation of motion leads to

$$\frac{d(U_1U_s)}{dx} I_1(\eta) - \frac{U_s}{B}\frac{d(U_1B)}{dx}\{\eta f - I_1(\eta) - \mu f(\mu)\} - U_s\frac{dU_s}{dx} I_2(\eta) + \frac{U_s}{B}\frac{d(U_sB)}{dx}\{fI_1(\eta) - I_2(\eta) + (f-f(\mu))\, I_\mu\} = \frac{U_s^2}{B}(g-g(\mu)), \tag{18}$$

where $f = f(y/B)$, $g = g(y/B)$, $\eta = y/B$; $\mu = \epsilon/B$ and is the smallest (non-dimensional) distance from the wall at which $f(\eta)$ accurately describes the mean velocity. Also

$$I_1(\eta) = \int_\mu^\eta f\,d\eta, \quad I_2(\eta) = \int_\mu^\eta f^2\,d\eta, \quad I_\mu = \int_0^\mu f\,d\eta.$$

For self-preserving flow, equation (18) must be identical in meaning for all x, that is coefficients of functions of x must be zero or in constant ratio. The relations

$$U_1 = aX^m = a(x-x_0)^m, \quad U_s = bX^m = b(x-x_0)^m, \quad B = cX = c(x-x_0) \tag{19a, b, c}$$

satisfy this condition and are therefore the conditions for self-preserving or precise equilibrium flow.

3.1. *Shear-stress distribution*

An explicit expression for the shear-stress distribution in these layers may be derived from equation (18) by substituting into it the self-preserving conditions (equations 19a, b, c) and separating out $\tau/\frac{1}{2}\rho U_1^2 (= -(2b^2/a^2)\,g)$. This equation involves the unknown $g(\mu)$ which can be replaced with an approximation following from the evaluation of equation (7) at $y = \mu B$, namely

$$g(\mu) \simeq -\frac{a^2}{2b^2}\left(c_f' + 2\alpha\mu\frac{B}{U_1^2}\right).$$

$B\alpha/U_1^2$ can be evaluated as $-mc$ using the self-preserving relations and this means that for $\mu = 0{\cdot}02$ the relationship can be written

$$g(\mu) \simeq \frac{a^2}{2b^2}(0{\cdot}04mc - c_f'). \tag{20}\dagger$$

Substitution of equation (20) into the expression for the shear stress leads to

$$\frac{\tau(\eta)}{\frac{1}{2}\rho U_1^2} = c_f' - \frac{0{\cdot}04m\gamma}{(a/b-\frac{1}{2})} - \frac{2\gamma}{(a^2/b^2)(a/b-\frac{1}{2})}\left\{\frac{a}{b}(3m+1)\,I_1(\eta) - (2m+1)\,I_2(\eta) - \frac{a}{b}(m+1)(\eta f - \mu f(\mu)) + (m+1)(fI_1(\eta) + fI_\mu - f(\mu)\,I_\mu)\right\}, \tag{21}$$

† The smaller the value of μ the more accurate this approximation becomes. It was found that provided μ was within the experimental range of 0·01–0·04 its actual value had a very minor effect on calculations described below where a value of 0·02 has been used throughout.

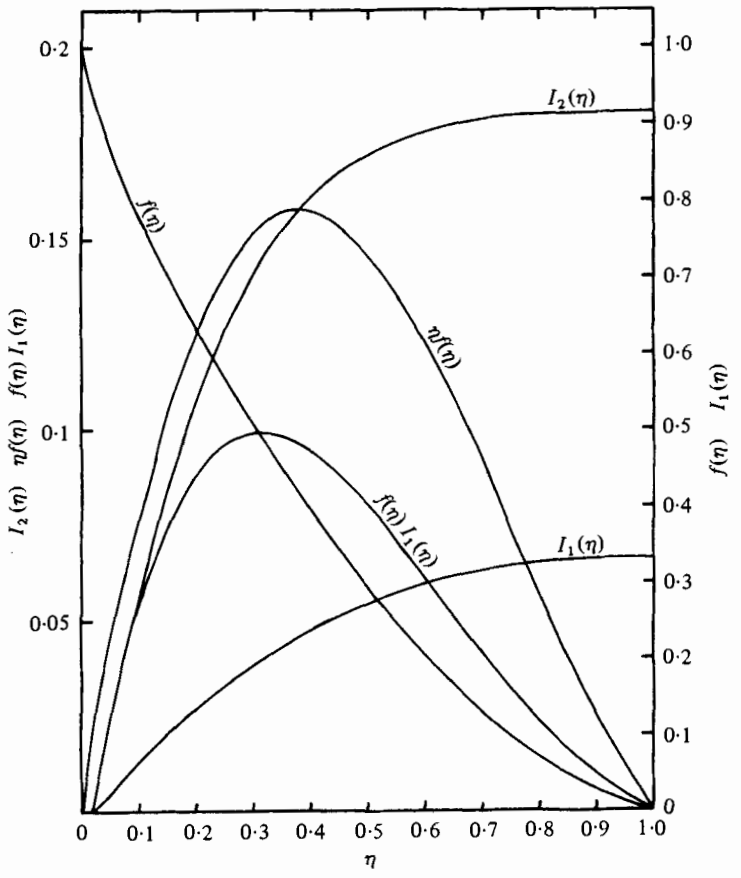

FIGURE 3. Functions of η.

where γ is the entrainment parameter defined (Townsend 1976) as

$$\gamma = \frac{U_1 + \frac{1}{2}u_0}{|u_0|}\frac{dl_0}{dx} = \left(\frac{a}{b} - \frac{1}{2}\right)c.$$

3.2. *Free-stream velocity variation*

A relation between m, the free-stream velocity variation exponent, and the velocity ratio U_1/U_s $(=a/b)$ can now be derived. For the particular case of $\eta = 1$, where $f(1) = 0$ and $\tau(1) = 0$, equation (21) can be rearranged to give

$$m = -\frac{\left\{\frac{a}{b}(I_1(1) + \mu f(\mu)) - I_2(1) - f(\mu)\,I_\mu\right\} - \frac{c_f'}{\gamma}\left(\frac{a^2}{2b^2}\left(\frac{a}{b} - \frac{1}{2}\right)\right)}{0{\cdot}02\frac{a^2}{b^2} + \frac{a}{b}(3I_1(1) + \mu f(\mu)) - 2I_2(1) - f(\mu)\,I_\mu}, \tag{22}$$

which defines m in terms of profile parameters and hence can assume a range of values depending on the velocity ratio U_1/U_s $(=a/b)$ and c_f'/γ. Functions of η appearing in the above equations are plotted in figure 3.

3.3. *Pressure-gradient parameters*

Clauser's original non-dimensional force ratio or pressure-gradient parameter may be written

$$\beta_c = -\delta^* \frac{U_1}{u_\tau^2}\frac{dU_1}{dx}.$$

It is argued here that, while this is the relevant parameter for flows in pressure gradients near zero where u_τ is relatively large and dominant, it is inappropriate for flows in moderate to strong pressure gradients where u_τ is relatively small and of minor importance. That is, the velocity scale of the logarithmic region is inappropriate for flows with small (or even disappearing) logarithmic regions and U_s, the velocity scale of the half-power region, should replace it. If this is the case the pressure-gradient parameter for layers in moderate to strong pressure gradient should be

$$\beta^* = -\delta^* \frac{U_1}{U_s^2}\frac{dU_1}{dx}, \tag{23}$$

and by using the definition $B = 2{\cdot}86\delta^* U_1/U_s$ and equations (19) for self-preserving flow β^* can be rewritten as

$$\beta^* = -mca/2{\cdot}86b, \tag{24}$$

which for the equilibrium layers analysed here must be constant.

3.4. *Existence limits for equilibrium layers*

There are three limiting conditions for the equilibrium layers analysed here. They are:

(i) $m < 0$, the condition for adverse-pressure-gradient flow;

(ii) $c_f' \geqslant 0$, the condition for attached flow;

(iii) $\tau_m \geqslant \frac{3}{2}\tau_0$, the condition for moderate to strong adverse-pressure-gradient flow in which the Schofield–Perry defect law applies.

Condition (ii) can be expressed in terms of flow parameters by substituting $c_f' = 0$ in equation (22), giving

$$m = -\frac{(a/b)\,(I_1(1)-\mu f(\mu))-I_2(1)-f(\mu)\,I_\mu}{0{\cdot}02(a^2/b^2)+(a/b)\,(3I_1(1)+\mu f(\mu))-2I_2(1)-f(\mu)\,I_\mu}. \tag{25}$$

Condition (iii) can also be made explicit by evaluating the general equation for the shear-stress profile (equation (21)) at the maximum stress condition, i.e. at $\eta = \eta_m = L/B$, where $\tau(\eta_m) = \tau_m$. This leads to

$$m = -J/K, \tag{26}$$

where

$$J = \frac{a}{b}I_1(\eta_m) - I_2(\eta_m) - \frac{a}{b}(\eta_m f(\eta_m) - \mu f(\mu)) + f(\eta_m)\,I_1(\eta_m) + f(\eta_m)\,I_\mu - f(\mu)\,I_\mu - \frac{a^2}{2\gamma b^2}\left(\frac{a}{b}-\frac{1}{2}\right)\left(c_f' - \frac{\tau_m}{\frac{1}{2}\rho U_1^2}\right),$$

$$K = 0{\cdot}02\frac{a^2}{b^2} + 3\frac{a}{b}I_1(\eta_m) - 2I_2(\eta_m) - \frac{a}{b}(\eta_m f(\eta_m) - \mu f(\mu)) + f(\eta_m)\,I_1(\eta_m) + f(\eta_m)\,I_\mu - f(\mu)\,I_\mu,$$

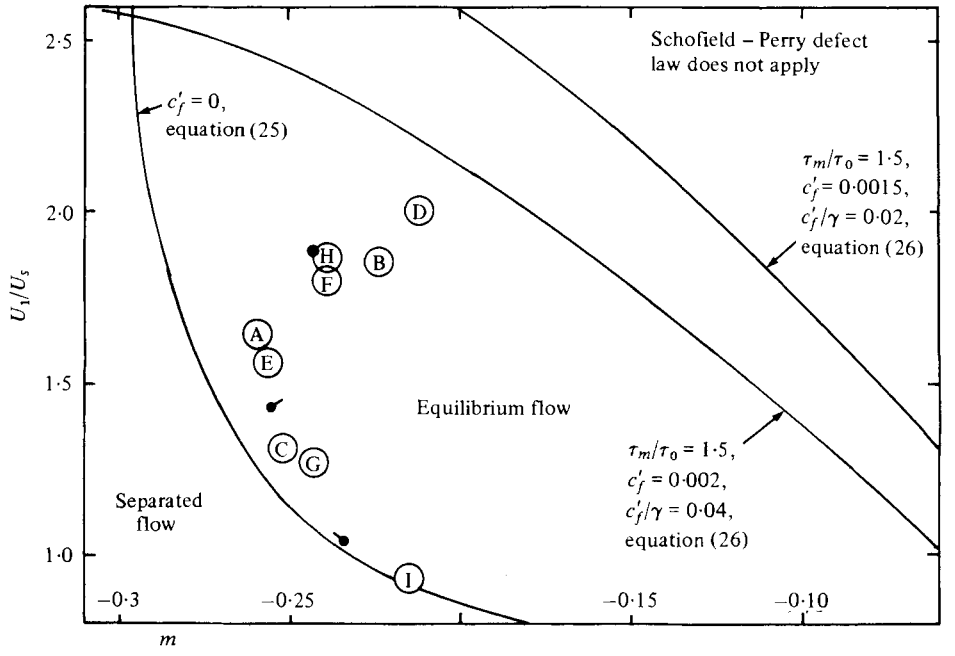

FIGURE 4. Limits of equilibrium flow. A, Ludwieg & Tillmann (1949), mild adverse pressure gradient; B, Clauser (1954), flow 1; C, Clauser (1954), flow 2; D, Bradshaw (1966); E, Bradshaw & Ferriss (1965); F, Bradshaw (1967); G, Stratford (1959), flow 5; H, Samuel (1973), flow 2; I, Stratford (1959), flow 6; ●, East *et al.* (1979), flow 5; ◐, East *et al.* (1979) flow 6; ◑, East *et al.* flow 7.

and at the limiting condition

$$\tau_m = \tfrac{3}{2}\tau_0 \quad \text{or} \quad U_m^2 = \tfrac{3}{2}u_\tau^2 \tag{27}$$

we have

$$J = \frac{a}{b}(I_1(\eta_m) - \eta_m f(\eta_m) + \mu f(\mu)) - I_2(\eta_m) + f(\eta_m) I_1(\eta_m) + f(\eta_m) I_\mu - f(\mu) I_\mu + \frac{c_f'}{\gamma}\frac{a^2}{4b^2}\left(\frac{a}{b} - \frac{1}{2}\right). \tag{28}$$

The value of η_m can be evaluated by using equation (13)

$$\eta_m = L/B = 64 U_m^2/U_s^2,$$

which with equation (27) can be rewritten

$$\eta_m = 48 c_f' a^2/b^2.$$

These equations define a space with co-ordinates m, a/b within which all equilibrium layers exist. Most of this space is shown in figure 4.

3.5. *Entrainment and skin friction*

For any equilibrium layer,

$$U_1/U_s = a/b = \text{const.}$$

by equations (19a, b). In addition the layer growth rate c is constant by equation (19c). Hence the entrainment rate of an equilibrium layer $\gamma(=(a/b - \frac{1}{2})c)$ is constant.

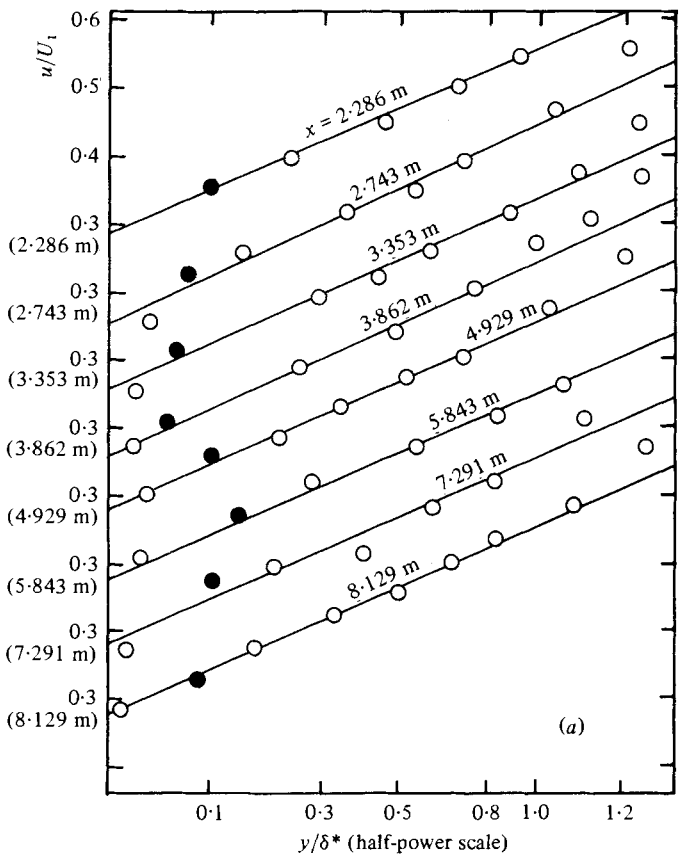

FIGURE 5. Half-power distributions of mean velocity. (*a*) ○, Clauser (1954), flow 2. (*b*) ○, Bradshaw (1966). ——, equation (11*b*); ●, data point closest to $0{\cdot}02\delta$.

As the exponent of free-stream velocity variation m of an equilibrium layer is constant and a/b, γ are also constant, equation (22) implies that c_f' is constant. It is important to note, however, that the wall shear stress enters the analysis through the wall-matching condition, equation (20), which is an approximation. If the analysis had been restricted to the outer 98 % of the layer in which the defect law was valid then it would yield the result that $\tau(\mu)/\frac{1}{2}\rho U_1^2$ is constant, which is a precise result. However, as $\tau(\mu)$ is not a useful parameter the analysis was extended to cover the whole layer by relating $\tau(\mu)/\frac{1}{2}\rho U_1^2 (= -2b^2 g(\mu)/a^2)$ to the wall shear via an approximation, equation (20), which can be written

$$c_f' \simeq 0{\cdot}04mc - 2g(\mu)\,(b^2/a^2) = \text{const.}$$

This equation implies that c_f' should be approximately constant in an equilibrium layer.

Approximately constant skin friction is a corollary of this theory and arises from the wall-matching condition. In contrast, the Rotta and Townsend analyses of equilibrium layers require a constant skin-friction coefficient as a condition of their existence.

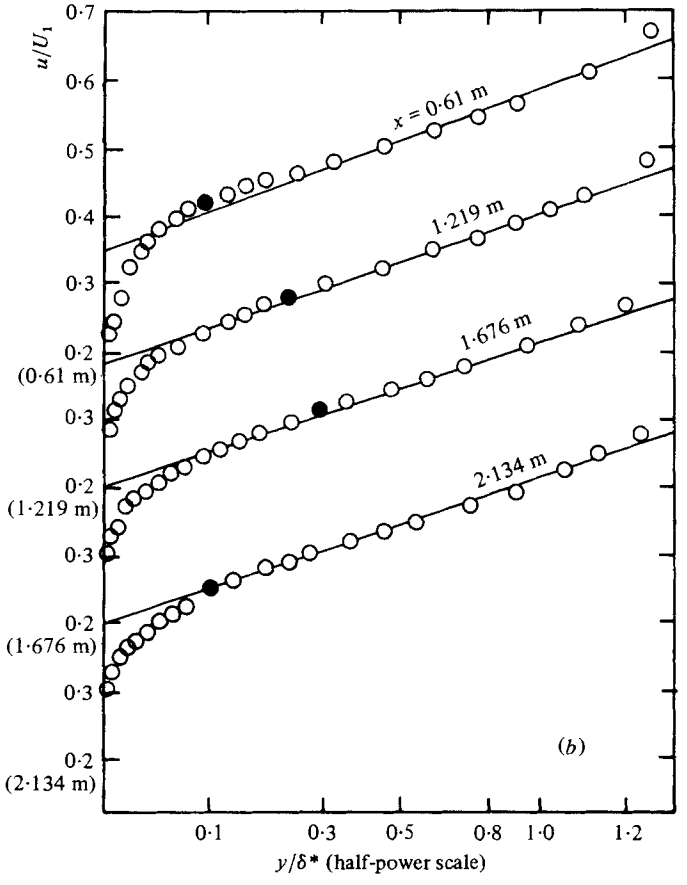

FIGURE 5b. For legend see p. 103.

4. Comparison with data

The literature was searched for attached flows in moderate to strong adverse pressure gradient in which the free-stream velocity distribution could be described by equation (19*a*). Twelve such flows were found, analysed and compared with the theoretical predictions. For nine of the flows (Ludwieg & Tillmann 1949, mild adverse-pressure-gradient flow; Clauser 1954, flows 1 and 2; Bradshaw & Ferriss 1965; Bradshaw 1967; Stratford 1959, flows 5 and 6; Samuel 1973, flow 2; Bradshaw 1966) full details of the results were available. These data will be referred to as the primary data. For the other three flows (East *et al.* 1979, flows 5, 6, 7) results were reported by East & Sawyer (1979) with some additional details given in East, Sawyer & Nash (1979). However, for these flows, tabulated data for only one profile per layer has been published in East *et al.* (1979). Thus, in order to compare these results with theoretical predictions it was necessary to make several assumptions. The accuracy of these assumptions is difficult to estimate and hence comparisons between the data of East *et al.* and theory cannot carry the same weight as comparisons involving the primary data.

Firstly, mean profiles were analysed to ensure they contained half-power distribu-

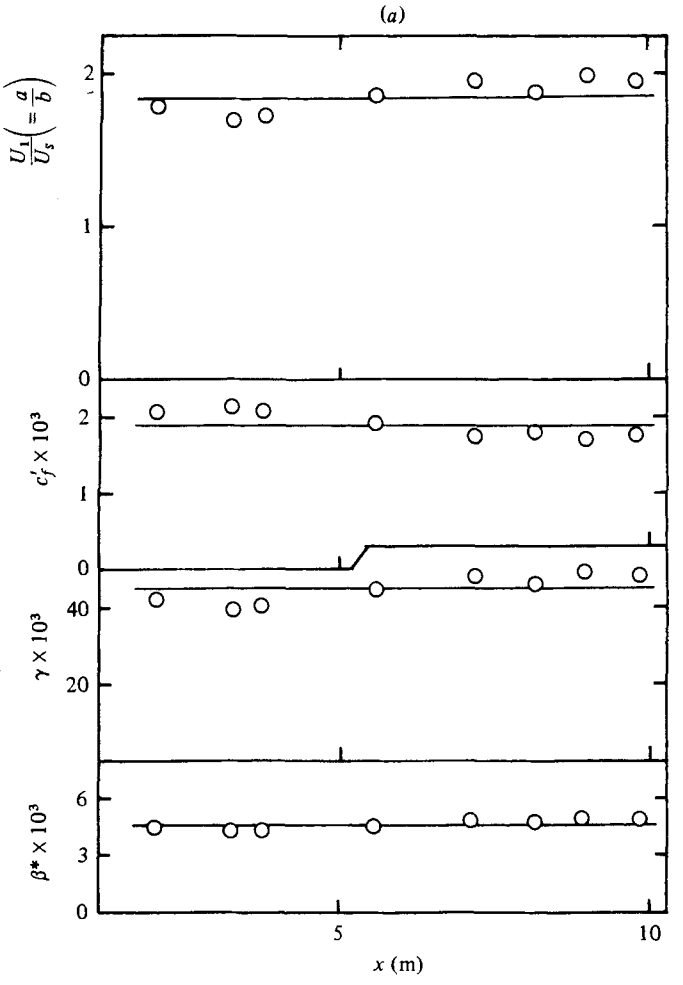

FIGURE 6. Parameters for equilibrium layers: (*a*) Clauser (1954), flow 1; (*b*) Stratford (1959), flow 5.

tions near the wall. All 49 profiles exhibited half-power distributions which extended to within a few per cent of layer thickness from the wall, as illustrated in figure 5. By comparing these distributions with the family of lines given by equation (11*b*) the velocity ratio U_1/U_s was determined for each profile. In the primary data it was found that $U_1/U_s = a/b$ was closely constant in each layer as required by theory.† Figure 6 shows some typical results.‡ Using these values of U_s the mean profiles were tested against the Schofield–Perry defect law (equation (12)) for the full layer. Typical results are shown in figure 7. Agreement between the data and equation (12) is good and typical of previous results for non-equilibrium layers (Schofield & Perry 1972; Perry & Schofield 1973; Simpson *et al.* 1977; Perry & Fairlie 1975; Samuel 1973).

As U_1/U_s was known, the integral layer thickness B could be calculated from its definition. In the nine primary data layers, variation of B with distance showed good

† For the data of East *et al.* it was assumed that in each of the three layers the single available value of a/b was the experimental average of the layer.

‡ Tabulated data is available from the author.

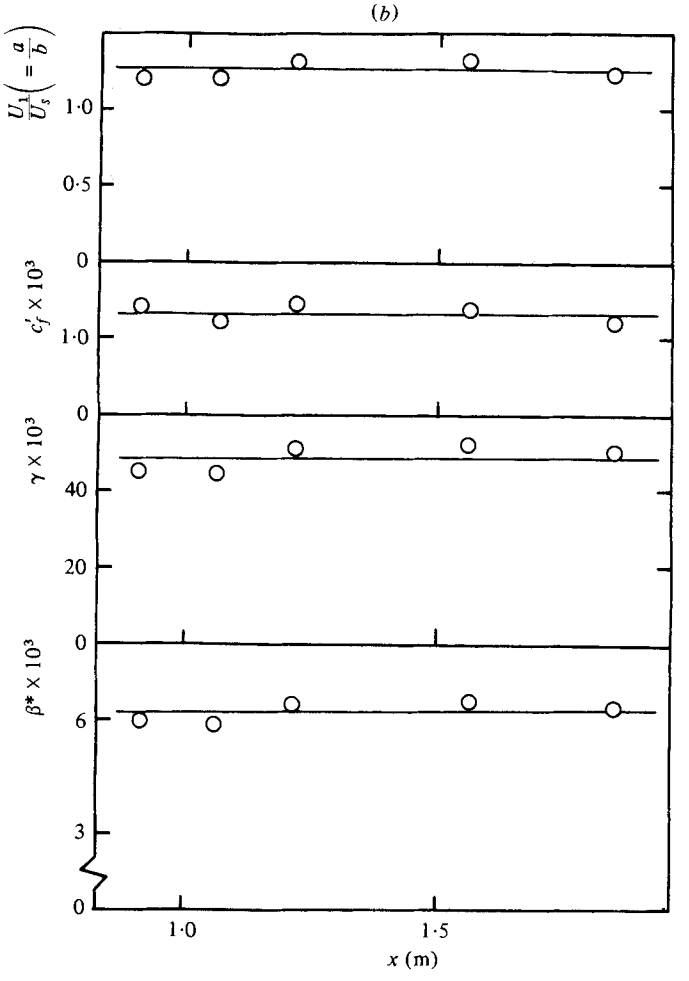

FIGURE 6b. For legend see p. 105.

linearity (see figure 8) and, therefore, the growth rates of the layers could be taken as constant. Thus the third of equations (19) was satisfied and with it all conditions for self-preserving or equilibrium flow for all the primary data. The variations of B in the layers of East *et al.* were unknown.

In each graph of B *versus* x in the primary data, the straight line of best fit determined values for c and x_0, the effective origin of each layer. Layer growth rates did not show the constancy between different layers assumed by Kader & Yaglom (1978). In fact, they showed considerable variation (0·03 to 0·10) around the value of 0·063 taken as constant by Kader & Yaglom (1978). East & Sawyer (1979) present results showing a fairly linear growth of momentum thickness with distance for their three layers. An estimate of c for these three layers was obtained from

$$c \simeq 2{\cdot}86 \frac{a}{b} H \, d\theta/dx,$$

where $H = \delta^*/\theta$. The accuracy of the estimate depends on the magnitude of dH/dx,

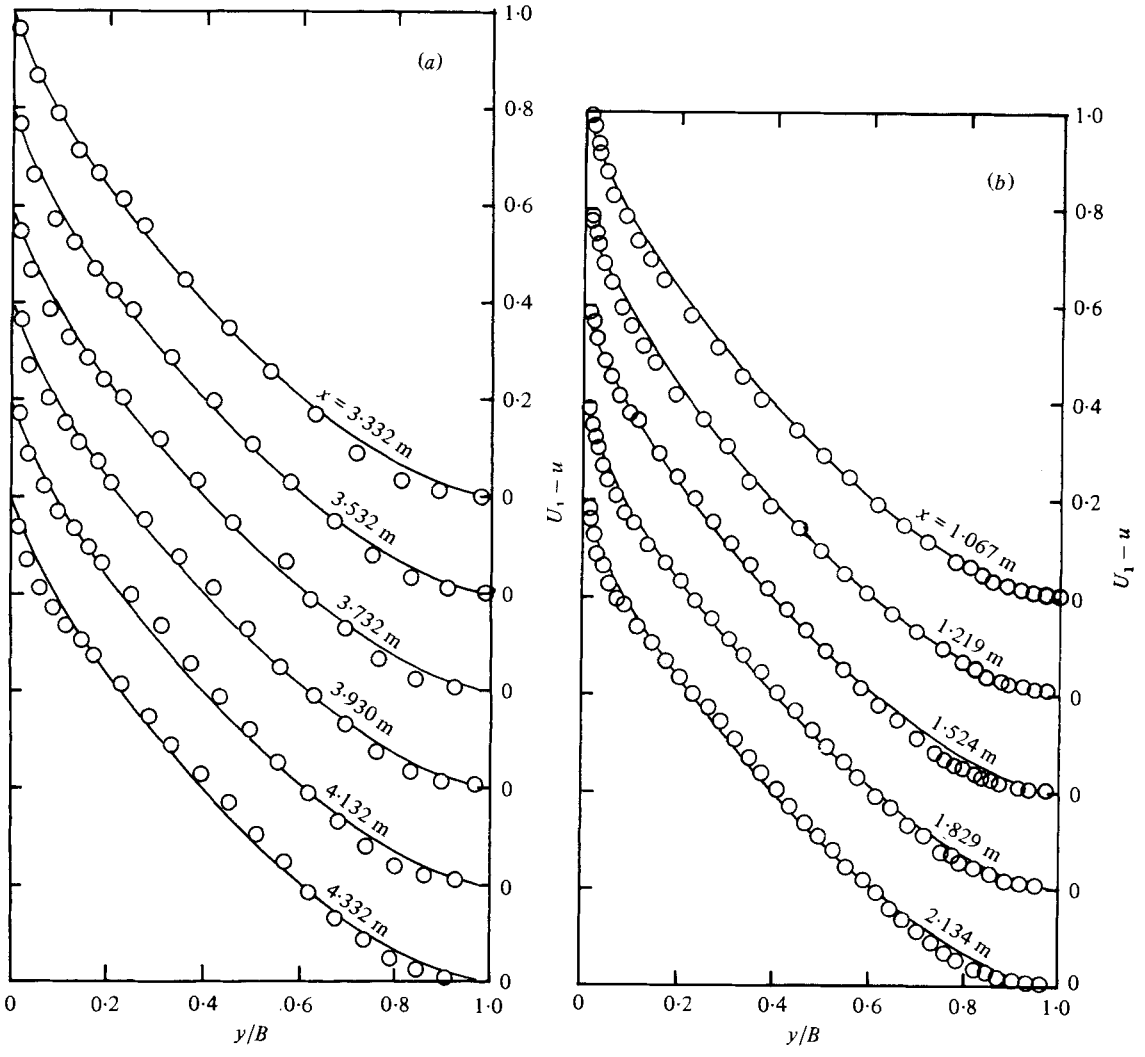

FIGURE 7. Mean velocity profiles on Schofield–Perry defect co-ordinates. (*a*) ○, Ludwieg & Tillmann (1949), mild adverse pressure gradient; (*b*) ○, Bradshaw (1967). ——, equation (12).

which has been assumed to be negligible but appears finite in the graphs presented by East *et al.* (1979). Another assumption involved here is that the effective origins (value of x_0) for θ and B coincide.

The entrainment and pressure-gradient parameters for the primary data were calculated and c_f' determined from Clauser charts (Clauser 1954). All these parameters were substantially constant in each layer (see figure 6) as required by the analysis. Skin-friction data for the layers of East *et al.* show a greater variation (see East & Sawyer 1979, p. 6).

Typical free-stream velocity variations with distance are shown for several layers in figure 9. Logarithmic co-ordinates have been used to show the linear logarithmic variation required by equation (19). Previously determined values of x_0 were used to calculate the abscissae $x - x_0$. All velocity variations have good linearity on these

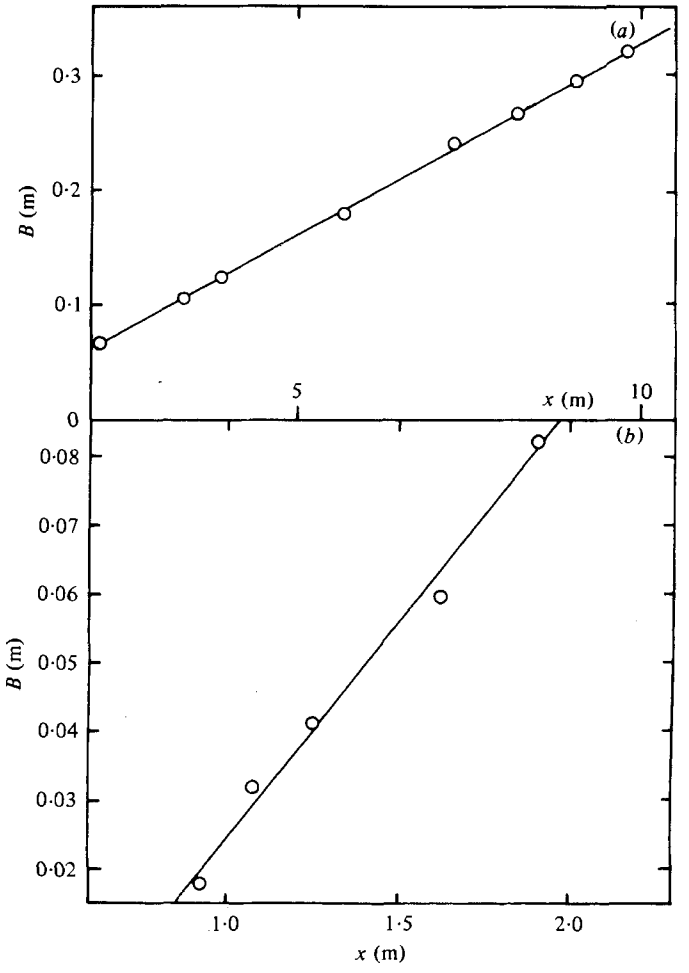

FIGURE 8. Growth of layer thickness. (*a*) ○, Clauser (1954), flow 1; (*b*) ○, Stratford (1959), flow 5. ——, line of best fit.

co-ordinates.† The lines joining points on the figure have slopes predicted theoretically by equation (22) and are in good agreement with the data, which is most encouraging.

This analysis of data enables the layers to be positioned on the *m versus* a/b diagram shown in figure 4. All layers fall within the limits set by equations (25) and (26), thus providing a degree of validation for the analysis. The positions of the primary data layers are represented on figure 4 by large circles because for each layer the experimentally derived values of c_f', γ and a/b show some (small) variation‡ and thus the position of the layer on m, a/b co-ordinates varies slightly with x. For each of the three layers of East *et al.*, data for only one streamwise station are available and hence these layers are represented on figure 4 by single solid dots.

The co-ordinate variables of figure 4 are the two major parameters that determine

† This fact is not significant as it was found that a fairly wide range of values for x_0 resulted in good linearity in the data on these log–log co-ordinates. For this reason x_0 was not determined from these plots.

‡ Variation of c_f', γ and a/b implies a variation in m via equation (22).

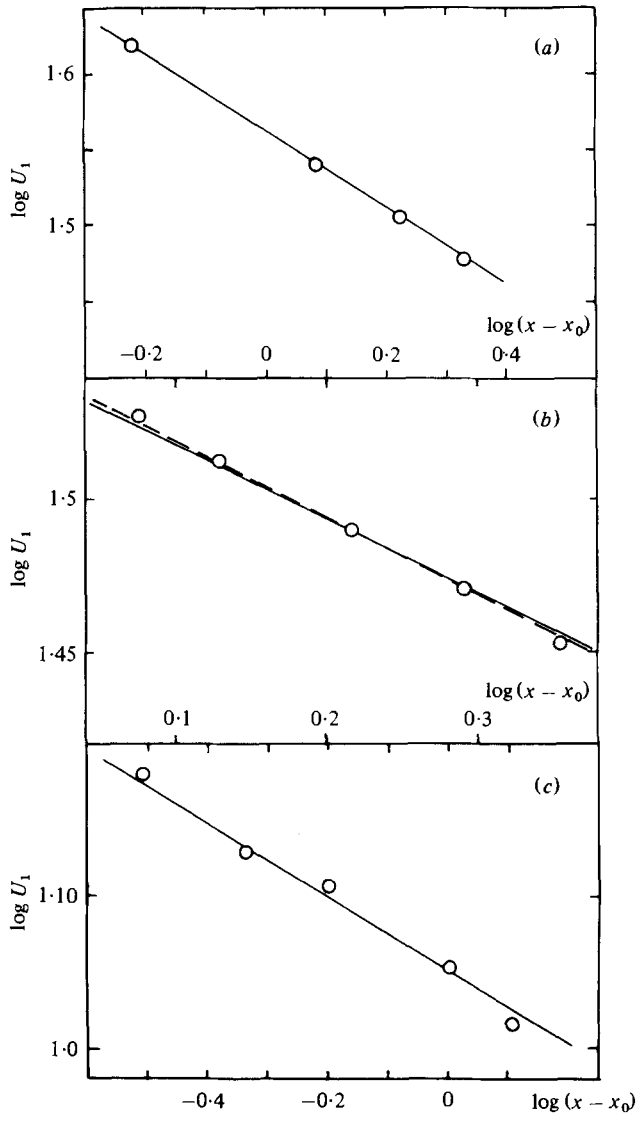

FIGURE 9. Free-stream velocity variation with distance. (*a*) ○, Bradshaw & Ferriss (1965). The slope given by Bradshaw & Ferriss agrees with that given by equation (22). (*b*) ○, Bradshaw (1967); — —, the slope given by Bradshaw. (*c*) ○, Stratford (1959), flow 5. ——, equation (22).

the development of an equilibrium layer. m is a measure of the severity of the pressure gradient applied to the layer which is the major boundary condition of the layer. Another boundary condition would be surface roughness.† The other ordinate of figure 4 U_1/U_s defines the shape of the mean velocity profile entering the equilibrium pressure gradient and hence is the layers' major initial condition. The other initial condition is the initial layer thickness which is shown later to have a minor effect on equilibrium layer development.

† Surface roughness would affect these equilibrium layers by increasing the wall shear stress and hence the shear stress $\tau(\mu)$.

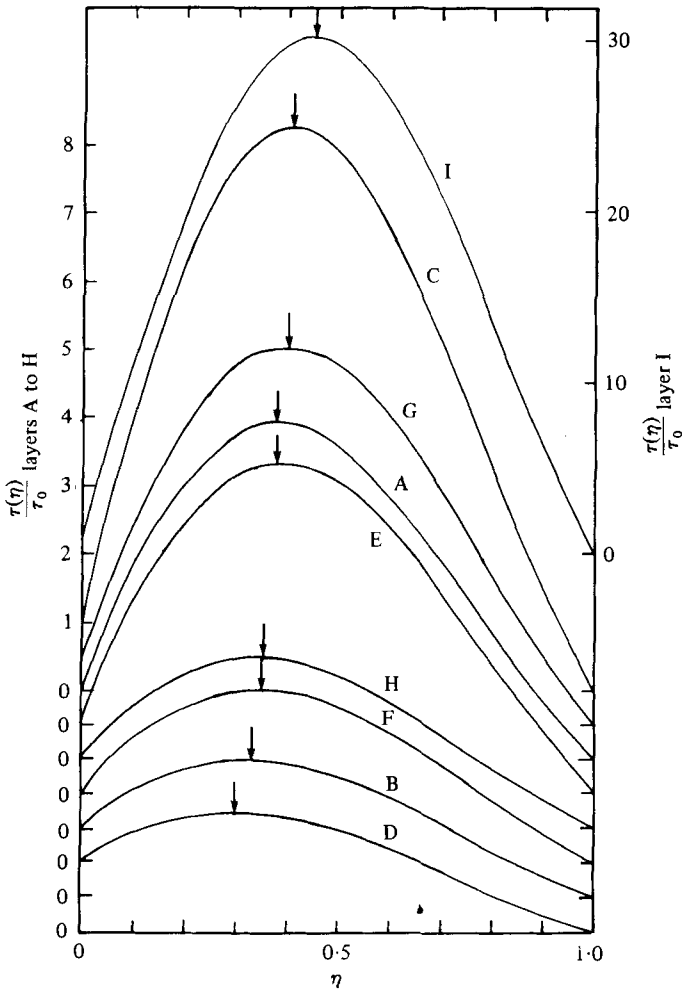

FIGURE 10. Equilibrium shear-stress profiles. A, Ludwieg & Tillmann (1949), mild adverse pressure gradient; B, Clauser (1954), flow 1; C, Clauser (1954), flow 2; D, Bradshaw (1966); E, Bradshaw & Ferriss (1965); F, Bradshaw (1967); G, Stratford (1959), flow 5; H, Samuel (1973), flow 2; I, Stratford (1959), flow 6. The arrows indicate the positions of τ_m. Note that the right-hand and left-hand scales differ.

Figure 4 implies that no equilibrium layer is possible in flows with m less than $-0{\cdot}3$, which is the limit given by Bradshaw (1967) from calculations using the method of Bradshaw *et al.* (1967). Head's conclusion that no equilibrium layer is possible for $m = -0{\cdot}35$ is also in agreement with this limit. Although Mellor & Gibson's (1966) conclusion that no equilibrium layer is possible for $m < -0{\cdot}23$ disagrees with this result, a possible reason for their conclusion is given below. The calculations of Townsend (1976) and East *et al.* (1979) give slightly lower limits for m that are Reynolds-number dependent.

Figure 4 implies that for a given boundary condition (given value for m) it is possible for a large range of equilibrium layers with different initial velocity ratios to exist. The experimentally observed layers plotted on figure 4 indicate that this occurs in practice. Thus Mellor & Gibson's (1966) conclusion that there is only a single sequence

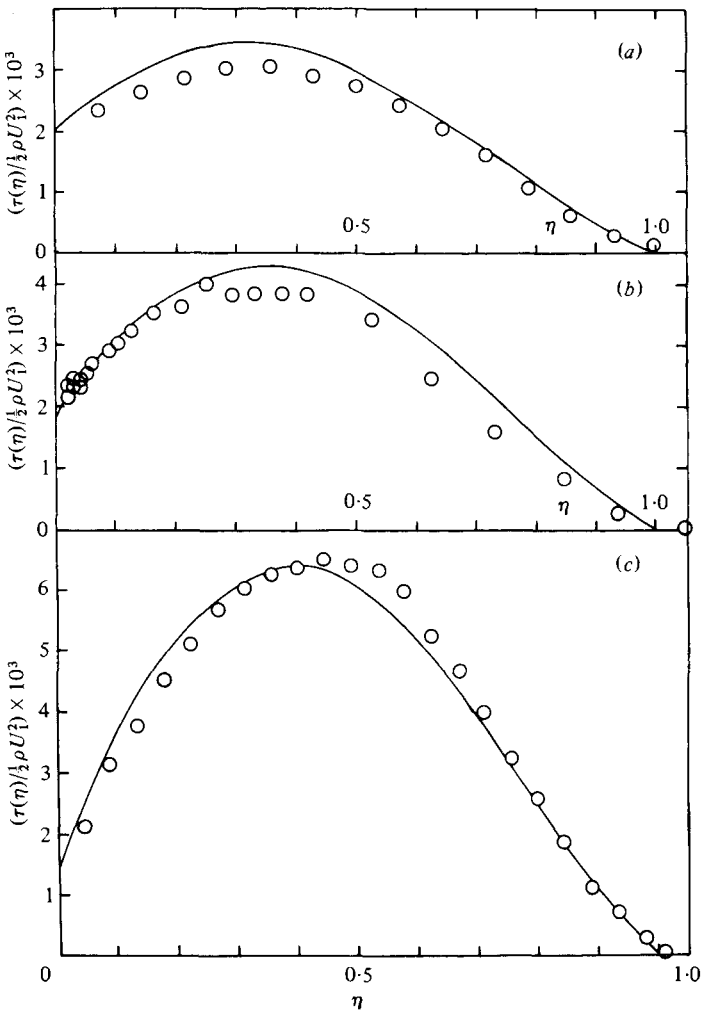

FIGURE 11. Equilibrium shear-stress profiles. (*a*) Moderate adverse pressure gradient (Bradshaw 1966); (*b*) medium adverse pressure gradient (Samuel 1973); (*c*) strong adverse pressure gradient (Bradshaw & Ferriss 1965); (*d*) moderate adverse pressure gradient (East *et al.* 1979, layer 5); (*e*) medium adverse pressure gradient (East *et al.* 1979, layer 6); (*f*) strong adverse pressure gradient (East *et al.* 1979, layer 7). ——, profile predicted by equation (21); ○, experimental data point.

of equilibrium layers is not supported by this analysis but Head's (1976) contention that a whole range of equilibrium layers exist for m near $-0{\cdot}25$ is supported.

Mellor & Gibson (1966) and Townsend (1960, 1976) have analysed the idealized Stratford flow, $\beta_c = \infty$, using different assumptions and methods. Both analyses give $m = -0{\cdot}23$ for this case whereas the present analysis would allow a large range in the boundary condition (along the $c_f' = 0$ curve in figure 4) to produce an ideal Stratford layer. Townsend employed a velocity ratio u_0/U_1 in which the velocity scale u_0 was determined by extrapolating an assumed mean profile down to the wall and was, therefore, somewhat similar to the velocity scale used in the present work. Townsend's analysis gives $u/U_1 = 0{\cdot}81$ at $m = -0{\cdot}23$, which is in fair agreement with figure 4,

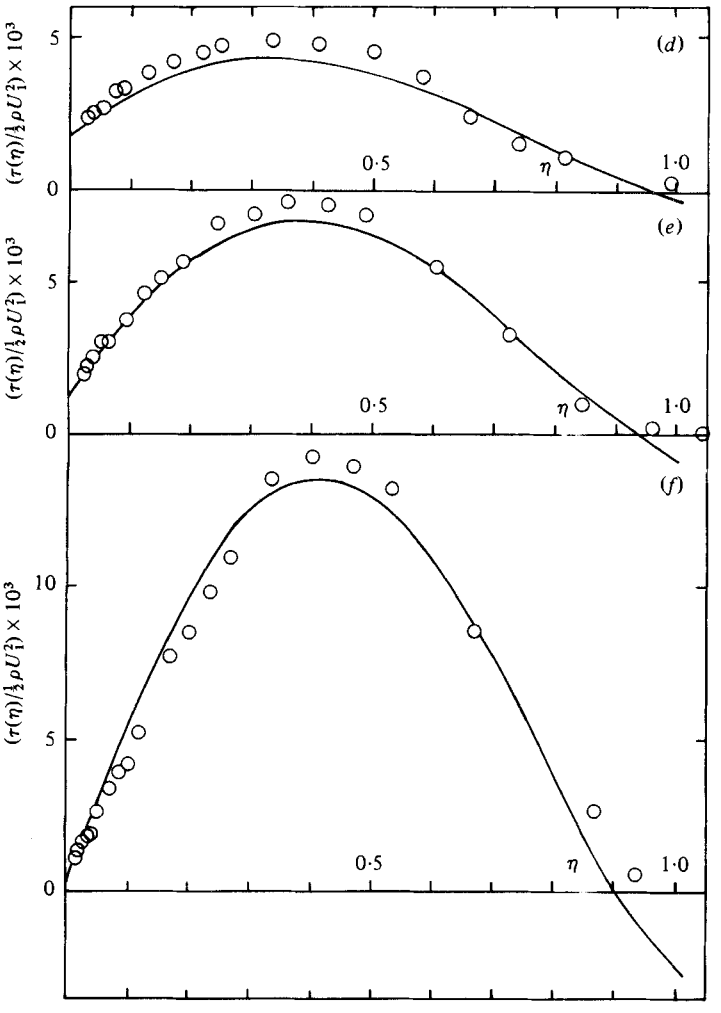

FIGURE 11 *d*, *e*, *f*. For legend see p. 111.

which gives $U_1/U_s \simeq 0{\cdot}94$ at $m = -0{\cdot}23$ for $c_f' = 0$. The actual Stratford flow nearest the condition $c_f' = 0$ is near this point with values $c_f' = 0{\cdot}4 \times 10^3$, $m = -0{\cdot}238$, $U_1/U_s = 0{\cdot}93$. Analytical results for Stratford's flows must, however, be treated with caution because, firstly, these flows are very close to separation and the normal stress terms which are significant near separation have been dropped from the equations of motion. Secondly, the two-dimensionality of Stratford's flows were suspect because of their large ratios of boundary-layer thickness to tunnel width.

4.1. *Shear-stress profiles*

Unlike other analyses of equilibrium boundary layers, the analysis presented here employs a general analytical expression for the mean flow profile (equation (12)) and hence it is possible using equation (21) to obtain the (invariant) shear-stress profile for any equilibrium layer from a knowledge of m, a/b, c_f' and c. As the experimentally derived values of c_f' and U_1/U_s showed some small variation in each layer the following calculations are based on average values. Values for m came from equation (22).

The predicted shear-stress profiles for the nine primary data layers are shown in figure 10. The profiles are forced to agree with the boundary condition at the wall where $\tau(0)/\frac{1}{2}\rho U_1^2 = c_f'$. However, in all cases the calculated value of shear stress at the free stream, where no agreement is forced, was zero to a very high order of accuracy. This agreement at $\eta = 1$ did not occur in the predicted shear-stress profiles for the three equilibrium layers of East *et al.* (see figure 11*d, e, f*). These inaccuracies are probably due to errors in the assumptions that were made in analysing these data. Figure 10 shows that η_m, the position of maximum shear stress, moves away from the wall as the ratio τ_m/τ_0 increases, varying from 0·3 for the limiting case of $\tau_m/\tau_0 = 1{\cdot}5$ to about 0·45 for the largest shear-stress ratio considered. This movement of τ_m was noted by East *et al.* (1979) in their experimental shear-stress profiles.

Fortunately shear-stress profiles in seven of the layers were measured by the authors allowing these predicted profiles to be compared with data. Figure 11 shows the comparisons.† For the primary data, figures 11(*a, b, c*) show comparisons for a moderate (Bradshaw 1966), medium (Samuel 1973) and strong (Bradshaw & Ferriss 1965) adverse-pressure-gradient layer. For these three layers the agreement is good and probably within the experimental uncertainty of measuring $\tau(\eta)$. The agreements could be marginally improved if the experimentally measured value of c_f' at the shear-stress measuring station was used rather than the average of the experimental values for the whole layer. These differences were, however, small. For the three profiles of East *et al.*, flows 5, 6, 7, shown in figures 11(*d, e, f*) the agreement is not as good. However, in these cases the predicted profiles are inaccurate (as $\tau(1)$ is not zero but substantially negative) owing to inaccuracies in the estimated values for m, a/b and particularly γ. Experience with these calculations suggest that a variation in parameters that will give $\tau(1) = 0$ will tend to increase τ_m and improve agreement with these data.

The remaining shear-stress measurements are by Bradshaw (1967) for a flow that developed initially in zero pressure gradient before approaching and entering a strong equilibrium adverse pressure gradient. The approach of the shear-stress profiles towards their new equilibrium form is shown in figure 12 where successive experimental shear-stress profiles are compared with both the shear-stress distribution the layer had in zero-pressure-gradient flow and the distribution predicted for the new equilibrium-pressure-gradient flow. The layer adjusts, firstly, near the wall where the time scale of the turbulence is small. Further modification of the shear-stress profile is slower and works outwards from the wall. In this case, the process is all but complete at the last recorded shear-stress profile where the agreement between experiment and theory is good.

4.2. *Mean-flow prediction*

The above account of equilibrium layers can be turned into a simple prediction method for layers in adverse-pressure-gradient flow. As well as being useful in itself this calculation procedure helps to resolve some of the disagreements in the literature on equilibrium layers.

We start by describing the mean velocity profile of these layers with the following set of expressions:

† The author is indebted to Professor Bradshaw for providing original data points for two of these layers.

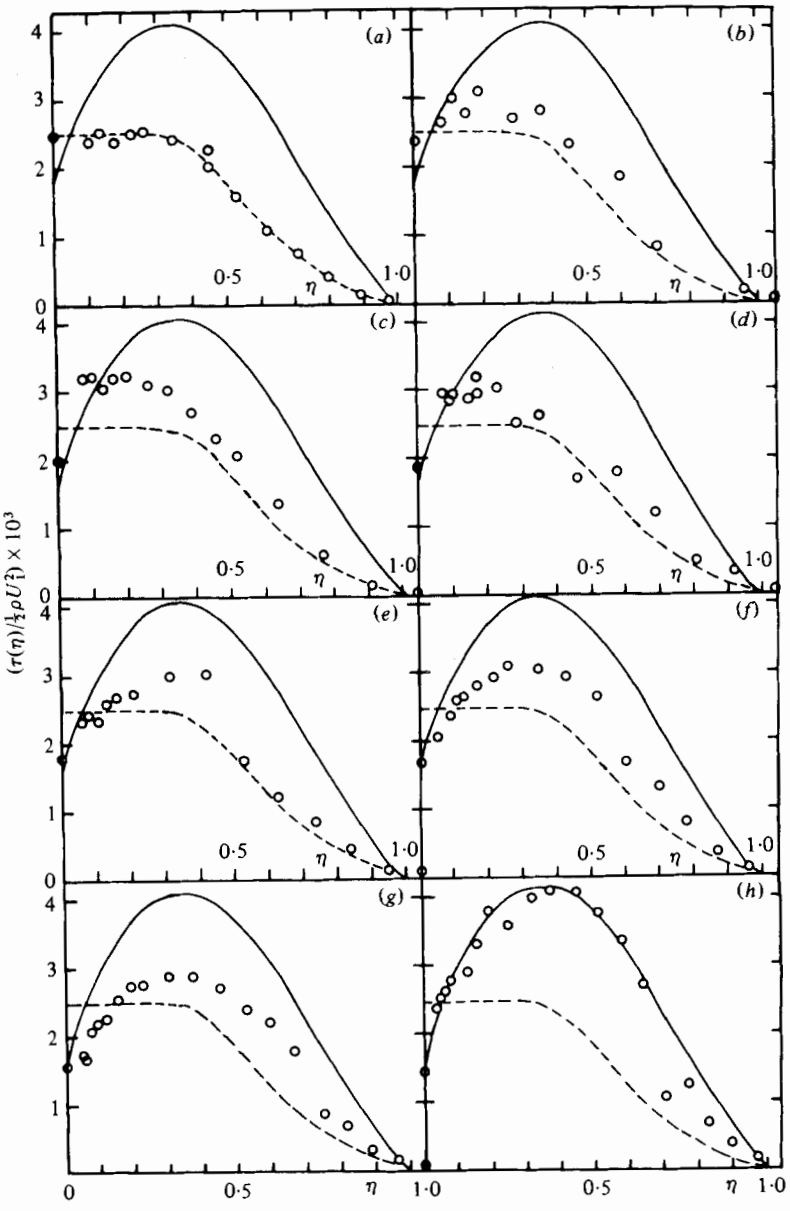

FIGURE 12. Shear-stress profiles of a boundary layer moving from zero pressure gradient to an equilibrium adverse pressure gradient for: (*a*) $x = 0{\cdot}61$ m; (*b*) $x = 0{\cdot}76$ m; (*c*) $x = 0{\cdot}91$ m; (*d*) $x = 1{\cdot}067$ m; (*e*) $x = 1{\cdot}219$ m; (*f*) $x = 1{\cdot}52$ m; (*g*) $x = 1{\cdot}829$ m; (*h*) $x = 2{\cdot}13$ m. ○, experimental data of Bradshaw (1967); ——, profile predicted by equation (21) for the equilibrium adverse-pressure-gradient layer.

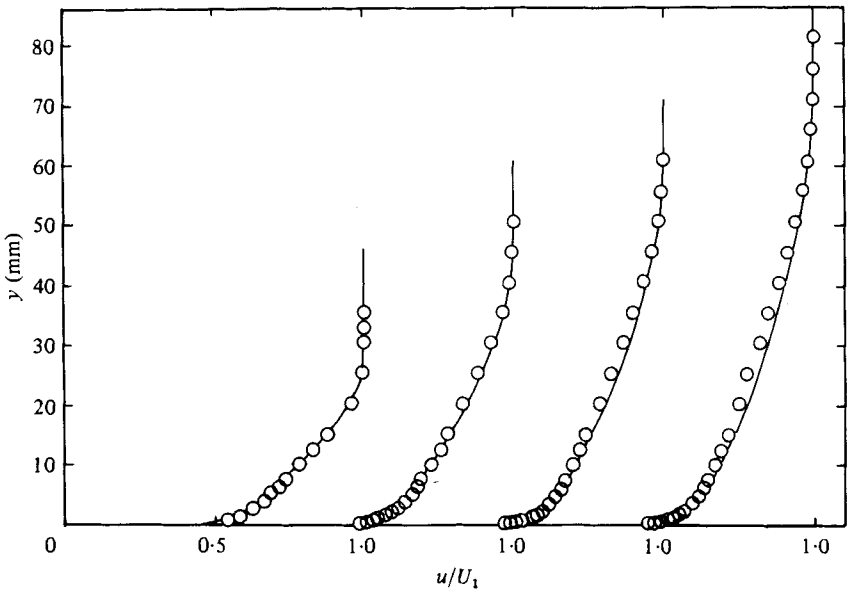

FIGURE 13. Mean velocity profiles from Bradshaw (1966) for '$a = -0{\cdot}15$'. ○, experimental data; ——, predicted profile.

(i) for the viscous sublayer from the wall ($y = 0$) to the intersection of the extrapolated linear and logarithmic distributions at $y = 10\nu/u_\tau$

$$u(y) = yu_\tau^2/\nu; \tag{29}$$

(ii) for the logarithmic region from $y = 10\nu/u_\tau$ to its junction with the outer defect law at $y = y_c\ (= 37{\cdot}1u_\tau^2 B/U_s^2)$

$$u(y) = 2{\cdot}44u_\tau \ln\frac{yu_\tau}{\nu} + 5{\cdot}0u_\tau; \tag{9}$$

(iii) for the outer defect law from $y = y_c$ to $y = B$

$$u(y) = U_1 - U_s + 0{\cdot}4U_s\left(\frac{y}{B}\right)^{\frac{1}{2}} + 0{\cdot}6U_s \sin\frac{\pi y}{2B}. \tag{12}$$

Prediction of a particular layer commences by matching initial and boundary conditions to the assumption of equilibrium flow in order to determine the characteristic constants of the flow m, c, x_0. The exponent m is obtained by fitting the free-stream velocity data to equation (19), which may be rewritten

$$\log U_1 = m\log(x - x_0) - \log a.$$

As initially x_0 is unknown it is taken as zero to give a first estimate of c. A corresponding estimate of c, the layer growth rate, is obtained using this estimate of m in equation (22) which can be rewritten as

$$\frac{u_\tau^2}{U_1^2} = c\left\{0{\cdot}02m + \frac{U_s}{U_1}(3m+1)I_1(1) - \frac{U_s^2}{U_1^2}(2m+1)I_2(1) + \frac{U_s}{U_1}(m+1)\mu f(\mu) - \frac{U_s^2}{U_1^2}(m+1)f(\mu)I_\mu\right\}. \tag{22}$$

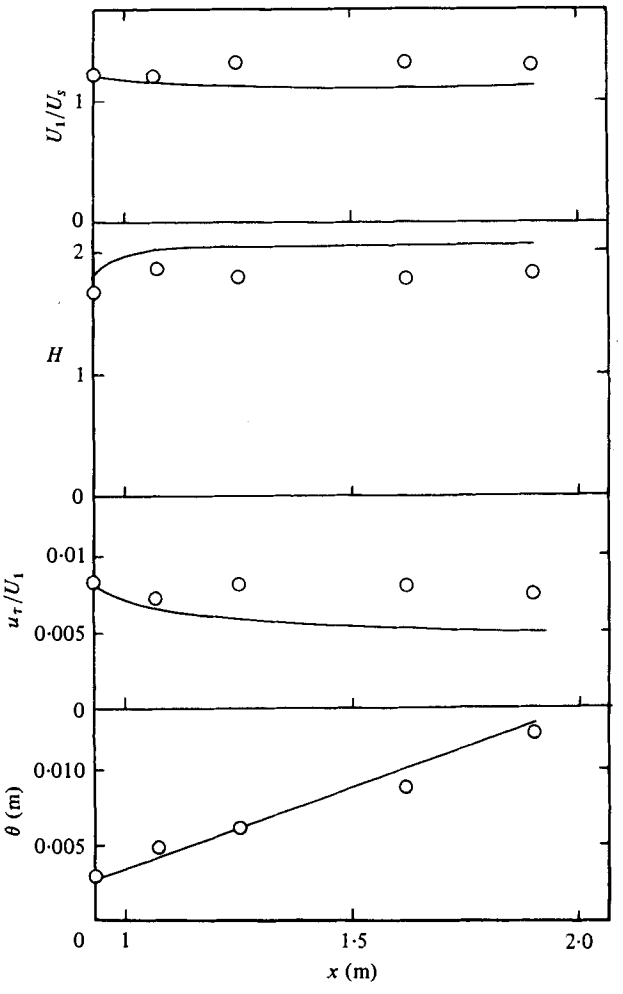

FIGURE 14. Mean-flow parameters from Stratford (1959), flow 5.
○, experimental data; ——, predicted variation.

Values for u_τ and U_s in this equation are obtained from the initial profile. This estimate of c and the initial layer thickness are substituted into equation (19b)

$$B = c(x - x_0) \tag{19b}$$

to give a new estimate for x_0. The process is then iterated until values for m, c and x_0 are stable.

To calculate any velocity profile downstream of the initial profile requires local values of u_τ, U_s and B. These are obtained by the simultaneous solution of three equations, two of which, equations (22) and (19b), were used above. The third equation is empirically based. It is derived from the observation reported by Perry & Schofield (1973) that the inner logarithmic law tangentially joins the outer defect law with no discernible blending or crossover region. Thus, equating the mean velocity

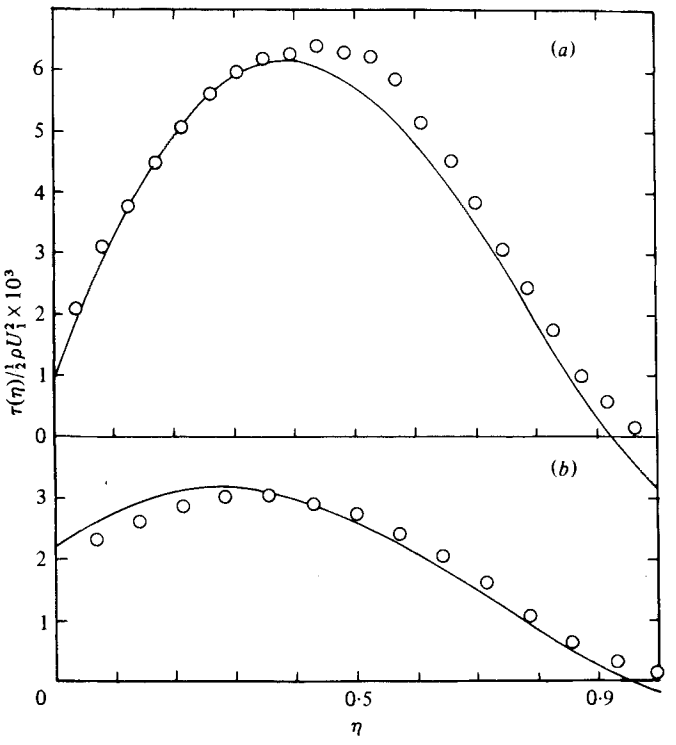

FIGURE 15. Shear-stress profiles from Bradshaw (1966) for: (*a*) $a = -0{\cdot}255$, (*b*) $a = -0{\cdot}15$. ○, experimental data; ——, predicted profile using predicted parameters in equation (21).

given by the outer law (equation (11*b*)) and the inner logarithmic law leads to

$$\frac{U_s}{U_1} = 1 - 8{\cdot}98\frac{u_\tau}{U_1} - 2{\cdot}44\frac{u_\tau}{U_1}\left[\ln\left(\frac{u_\tau}{U_s}\right)^2 + \ln\frac{u_\tau}{U_1} + \ln\frac{BU_1}{\nu}\right]. \tag{30}$$

The last term in this equation involves the logarithm of the Reynolds number based on layer thickness. Values of u_τ and U_s obtained from the simultaneous solution of equations (22) and (30) will therefore vary (slowly) as $\ln(BU_1/\nu)$ varies. These variations in u_τ and U_s are once again the result of an (empirical) matching of the outer equilibrium flow with the wall flow. Similar weak Reynolds-number dependences appear in the calculations of Townsend (1976), Mellor & Gibson (1966), and East *et al.* (1979).

This calculation procedure has been applied to the nine primary data layers.† Figure 13 shows typical comparisons between predicted and measured mean velocity profiles. Figure 14 shows similar comparisons for the velocity ratios U_1/U_s, u_τ/U_1, form factor δ^*/θ and momentum thickness. At the 1968 conference on computation of turbulent boundary layers (Kline *et al.* 1968) comparisons of the type shown in figure 14 were considered the more searching test of a prediction method. The agreements obtained here, for the nine layers, were as good or better than the best obtained by any of the methods presented at the Stanford Conference for these layers. Of course

† The data of East *et al.* (1979) were excluded because only one mean velocity profile was available for each layer.

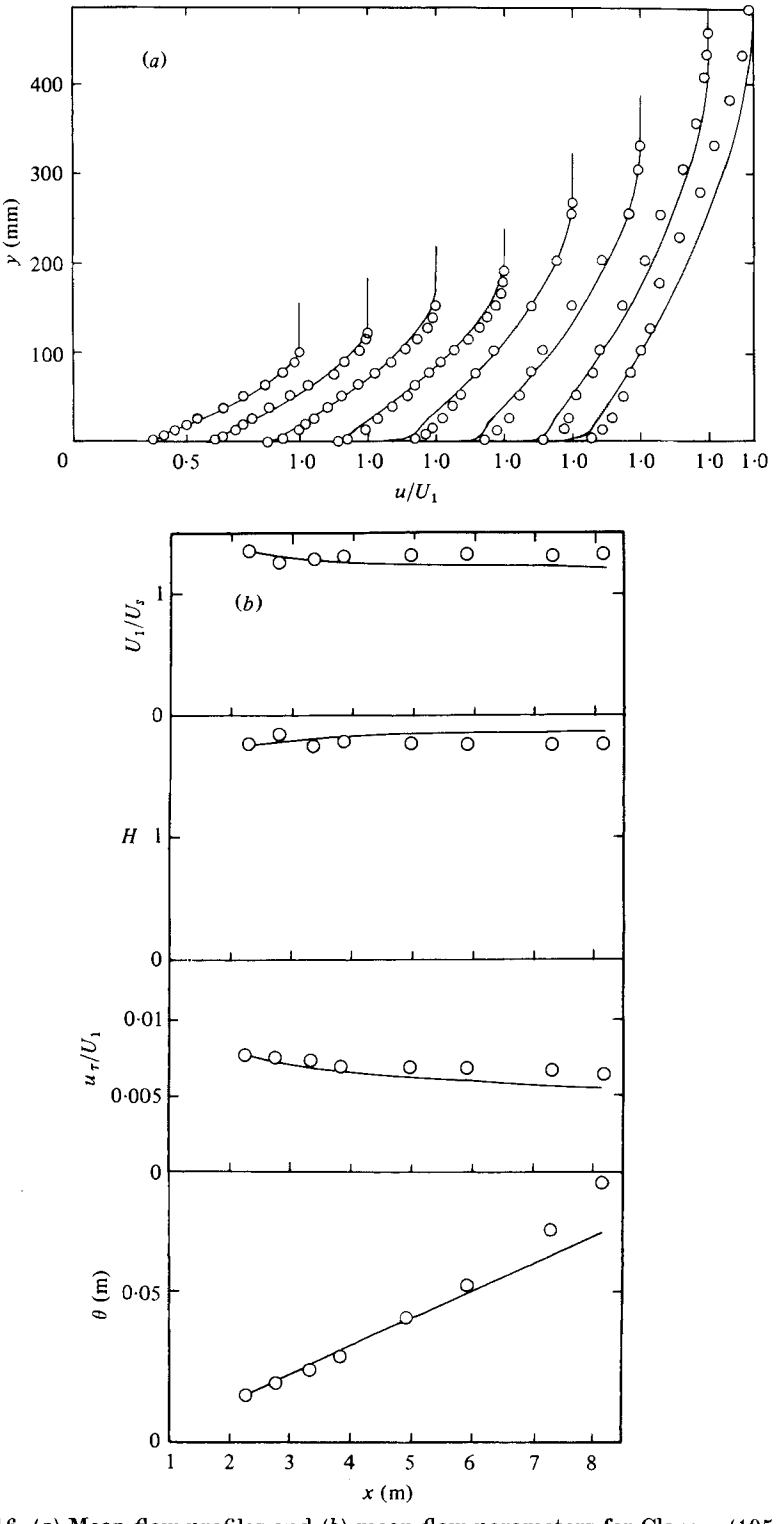

FIGURE 16. (*a*) Mean-flow profiles and (*b*) mean-flow parameters for Clauser (1954), flow 2. ○, experimental data; ——, predicted variation.

the present method can only apply to layers in moderate to strong adverse pressure gradients. However, unlike other prediction methods the present method can predict the shear-stress profiles across a layer. Examples of predicted shear-stress profiles using predicted parameters in equation (21) are shown in figure 15. The agreement obtained between predicted and measured profiles is not as good as that obtained previously using equation (21) with measured values of the parameters (see figure 11). However, these shear-stress profiles are sufficiently accurate to give a useful prediction.

This calculation method could be extended to adverse-pressure-gradient layers in moving equilibrium. A layer in moving equilibrium has boundary conditions that change continuously and relatively slowly so that the layer can be considered as continuously moving from one equilibrium state to another and at any position in its development to be locally in equilibrium. In such a layer the characteristic constants m, c, x_0 will have to be successively redetermined as the calculation proceeds downstream. In each of these redeterminations of m, c and x_0 a profile predicted by the method will be used as the initial condition for the next portion of equilibrium flow.

In the calculation procedure the simultaneous solution of equations (22) and (30) give two solutions for every profile: a 'type-1' solution in which a moderate velocity defect is associated with a large wall stress, and a 'type-2' solution in which a very large velocity defect is associated with a much lower wall shear stress. The relevant solution for any layer is the one that gives values of U_1/U_s (and u_τ/U_1) that agree with the initial conditions. Of the layers analysed here four had type-1 solutions and the remaining five had type-2 solutions. Townsend's (1960, 1976) analysis also predicts two possible equilibrium layers for a single set of initial and boundary conditions. His analysis of the Clauser (1954) layer 1 shows it to be a type-1 solution which agrees with the present analysis. However, for the Clauser (1954) layer 2 his analysis shows the layer to be in 'an area of ambiguous development and its observed development is not described by this theory' (Townsend 1960). Figure 16 shows that this layer is adequately described by the present theory and is a type-2 solution. Townsend (1976, p. 276) gives $m = -0{\cdot}25$ as the lower limit above which there is only one solution with positive u_τ. However, the present results† show that the Stratford (1959) flows 5 and 6 and the Clauser (1954) flow 1 have values of m greater than $-0{\cdot}25$ and yet have two solutions with positive values of u_τ.

The theoretical limit for only one attached solution can be obtained simply by substituting the condition $u_\tau = 0$ into equation (30). This yields $U_s = U_1$, which is the condition of the outer law extending to the wall (i.e. no logarithmic layer) and is an approximate result as the sublayer has not been considered. Substitution of $U_1 = U_s$ into equation (22) yields $m = -0{\cdot}23$ as the upper limit for two attached solutions.‡ The primary data contain only one layer in which $m > -0{\cdot}23$, the flow by Bradshaw (1966) '$a = -0{\cdot}15$', and the present calculation method did give only one attached solution. Bradshaw's (1966) criticism and explanation of the two solutions given by Townsend's analysis does not apply to this analysis. The present analysis does use the same assumption that Townsend used, that there is a smooth junction between the

† Detailed prediction results for the primary data layers are available from the author.

‡ It is possible that Mellor & Gibson's (1966) conclusion of a single series of equilibrium layers terminating at $m = -0{\cdot}23$ is the result of their analysis yielding only the type-2 solution equilibrium layers.

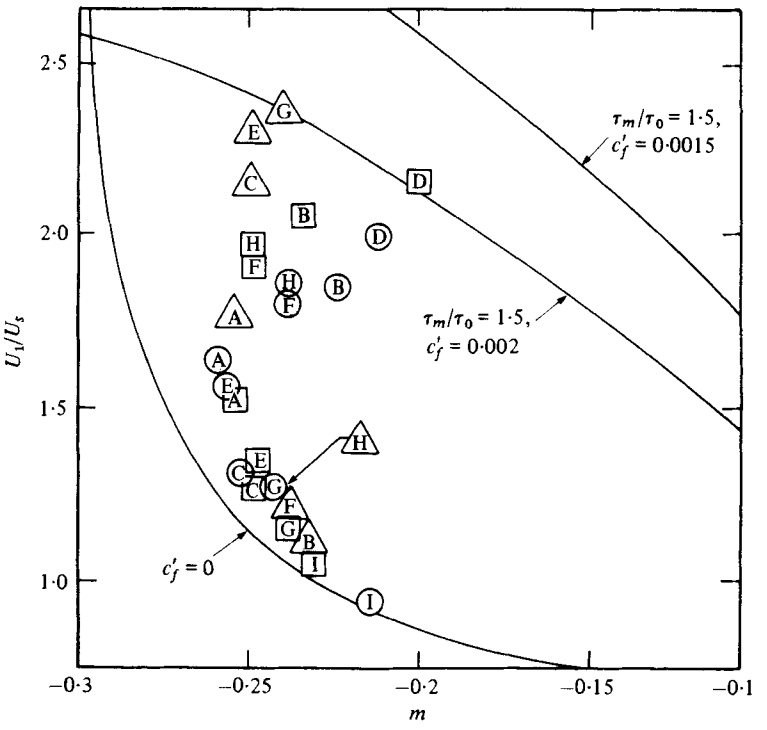

FIGURE 17. Equilibrium layers (primary data). ○, actual equilibrium layer; □, predicted equilibrium layer; △, alternative equilibrium layer. Letters identify layers listed in caption to figure 4.

mathematical expressions for the inner and outer regions of the layer. However, in this case it has been demonstrated empirically by Perry & Schofield (1973) and Schofield & Perry (1972) that the assumed models for the two regions join tangentially with no blending region and that these mathematical expressions accurately describe the experimental data in the junction region.

The equilibrium layers that have been predicted are plotted on m, U_1/U_s co-ordinates in figure 17 and are all close to the positions of the actual observed equilibrium layers. The second solutions for alternative equilibrium layers are also shown. They are generally well removed from the measured layers but are within the limits for equilibrium layers. Only the second solution for the Stratford flow 6 fell outside the limits and is not shown in the figure.

Finally, we can give an interpretation of Head's (1976) calculations for layers with $m = -0{\cdot}15, -0{\cdot}255$. For the $m = -0{\cdot}15$ case, Head's calculations suggested that only one equilibrium layer was possible, irrespective of the initial layer thickness. The calculations consisted of a series of predictions for layer development with differing initial layer thickness but with set boundary conditions ($m = -0{\cdot}15$) and set initial conditions (initial value of δ^*/θ held constant). The calculations showed several boundary-layer developments apparently converging on a single equilibrium condition but were not continued far enough to be conclusive. In the present theory for flows with m near $-0{\cdot}15$ a single (attached) solution is expected for a given initial boundary-layer shape U_1/U_s. Increasing the initial layer thickness causes m, c and x_0

to change and layer thicknesses downstream of the initial position to increase. The effects on the two solution curves, equations (22) and (30), are in opposite directions and to a certain extent self-cancelling. However, the net effect is to lower slightly the solution values of u_τ and U_s. Thus this conclusion of Head may be correct to a first approximation only.

For the case of $m = -0{\cdot}255$ and an invariant initial profile shape, Head's calculations predict that a range of equilibrium layers are generated for different initial layer thicknesses, and that, for initial layer thicknesses greater than twice the actual value, the layer will separate before an equilibrium layer can be established. As $m < -0{\cdot}23$ the present analysis predicts two possible layers, only one of which will have the correct velocity ratio. Calculations for this case show that the values of u_τ and U_s change very little for a doubling of the initial layer thickness. Furthermore, u_τ did not become negative even for initial thicknesses one hundred times the actual value. Thus, this solution of Head's is not supported and indeed it is difficult to envisage a physical mechanism to explain Head's result of a separation induced in a layer by increasing its initial thickness while holding other non-dimensional ratios constant.

5. Conclusions

Analysis of equilibrium boundary layers using the length and velocity scales of Schofield and Perry have several significant advantages. Firstly, the scales do not need modification to describe near-separating layers in very severe pressure gradients. Secondly, the Schofield–Perry defect law, which is the basis of the analysis, has the same analytical expression for all medium to strong adverse-pressure-gradient layers and this allows shear-stress profiles of equilibrium layers to be quite accurately predicted. Thirdly, the limits of the Schofield–Perry theory can be translated into limits in the initial and boundary conditions within which these equilibrium layers will be produced. These limits are consistent with results from experimental layers and with several previous calculations using approximate closure hypotheses.

This work gives a unified description of equilibrium layers in moderate to strong adverse pressure gradients. The majority of results by other authors are consistent with this description and in a few cases apparent disagreements between authors can be resolved by reference to it. Specifically the present analysis is in agreement with the following particular conclusions:

(i) no equilibrium layer is possible for $m < -0{\cdot}3$ (Head 1976; Bradshaw 1966);

(ii) for a given set of initial and boundary conditions two types of equilibrium layer are possible, one with large wall stress and the other with a lower wall stress (Townsend 1960; East *et al.* 1979) – both types of layer have been observed;

(iii) for equilibrium flows in which $m > -0{\cdot}23$ only one (attached) equilibrium layer is possible (Head 1976; Mellor & Gibson 1966);

(iv) for a given free-stream boundary condition within the equilibrium range ($-0{\cdot}3 < m < \sim -0{\cdot}1$) a wide range of equilibrium layers are possible (Head 1976). For a given value of m the particular equilibrium layer that will develop depends on the initial conditions, mainly the initial velocity ratio.

REFERENCES

BRADSHAW, P. 1966 *N.P.L. Aero. Rep.* no. 1184. (See also *J. Fluid Mech.* **29**, 1967, 625.)

BRADSHAW, P. 1967 *N.P.L. Aero. Rep.* no. 1219.

BRADSHAW, P. & FERRISS, D. H. 1965 *N.P.L. Aero. Rep.* no. 1145.

BRADSHAW, P., FERRISS, D. H. & ATWELL, N. P. 1967 *J. Fluid Mech.* **28**, 593.

COLES, D. E. & HIRST, E. A. 1968 *A.F.O.S.R.–I.F.P. Stanford Conf. on Turbulent Boundary Layer Prediction*, vol. 2.

CLAUSER, F. H. 1954 *J. Aero. Sci.* **21**, 91.

EAST, L. F. & SAWYER, W. G. 1979 *AGARD Conf. Proc.* 271.

EAST, L. F., SAWYER, W. G. & NASH, C. R. 1979 *R.A.E. Tech. Rep.* no. 79040.

EAST, L. F., SMITH, P. D. & MERRYMAN, P. J. 1977 *R.A.E. Tech. Rep.* no. 77046.

FAIRLIE, B. D. 1973 Ph.D. thesis, University of Melbourne.

HAMA, F. R. 1954 *Trans. Soc. Nav. Arch. Mar. Eng.* **62**, 333.

HEAD, M. R. 1976 *J. Fluid Mech.* **73**, 1.

KADER, B. A. & YAGLOM, A. M. 1978 *J. Fluid Mech.* **89**, 305.

KLEBANOFF, P. S. 1954 *NACA TN* 3178.

KLINE, S. J., MORKOVIN, M. V., SOVRAN, G. & COCKRELL, D. J. 1968 *A.F.O.S.R.–I.F.P. Stanford Conf. on Turbulent Boundary Layer Prediction*, vol. 1.

LUDWIEG, H. & TILLMANN, W. 1949 *Ing-Arch.* **17**, 288. (Transl. *NACA TM* 1285, 1950.)

MELLOR, G. L. & GIBSON, D. M. 1966 *J. Fluid Mech.* **24**, 225.

PERRY, A. E. & FAIRLIE, B. D. 1975 *J. Fluid Mech.* **69**, 657.

PERRY, A. E. & SCHOFIELD, W. H. 1973 *Phys. Fluids* **16**, 2068.

ROTTA, J. C. 1962 *Prog. Aero. Sci.* **2**, 3.

SAMUEL, A. E. 1973 Ph.D. thesis, University of Melbourne.

SAMUEL, A. E. & JOUBERT, P. N. 1974 *J. Fluid Mech.* **66**, 481.

SCHOFIELD, W. H. & PERRY, A. E. 1972 *A.R.L. Mech. Eng. Rep.* no. 134.

SIMPSON, R. L., STRICKLAND, J. H. & BARR, P. W. 1977 *J. Fluid Mech.* **79**, 553.

STRATFORD, B. S. 1959 *J. Fluid Mech.* **5**, 1, 17.

TOWNSEND, A. A. 1956*a* *J. Fluid Mech.* **1**, 561.

TOWNSEND, A. A. 1956*b* *The Structure of Turbulent Shear Flow*. Cambridge University Press.

TOWNSEND, A. A. 1960 *J. Fluid Mech.* **8**, 143.

TOWNSEND, A. A. 1961*a* *J. Fluid Mech.* **11**, 97.

TOWNSEND, A. A. 1961*b* *J. Fluid Mech.* **12**, 536.

TOWNSEND, A. A. 1965*a* *J. Fluid Mech.* **22**, 773.

TOWNSEND, A. A. 1965*b* *J. Fluid Mech.* **23**, 767.

TOWNSEND, A. A. 1976 *The Structure of Turbulent Shear Flow*, 2nd edn. Cambridge University Press.

YAGLOM, A. M. 1979 *Ann. Rev. Fluid Mech.* **11**, 505.